Benchmarking density-functional theory calculations of NMR shielding constants and spin–rotation constants using accurate coupled-cluster calculations

Andrew M. Teale,[1,2] Ola B. Lutnæs,[1] Trygve Helgaker,[1] David J. Tozer,[3] and Jürgen Gauss[4]

[1]*Department of Chemistry, Centre for Theoretical and Computational Chemistry, University of Oslo, P.O. Box 1033 Blindern, N-0315 Oslo, Norway*
[2]*School of Chemistry, University of Nottingham, University Park, Nottingham, NG7 2RD, United Kingdom*
[3]*Department of Chemistry, Durham University, South Road, Durham, DH1 3LE, United Kingdom*
[4]*Institut für Physikalische Chemie, Universität Mainz, D-55099 Mainz, Germany*

(Received 3 October 2012; accepted 6 December 2012; published online 11 January 2013)

Accurate sets of benchmark nuclear-magnetic-resonance shielding constants and spin–rotation constants are calculated using coupled-cluster singles–doubles (CCSD) theory and coupled-cluster singles–doubles–perturbative-triples [CCSD(T)] theory, in a variety of basis sets consisting of (rotational) London atomic orbitals. The accuracy of the calculated coupled-cluster constants is established by a careful comparison with experimental data, taking into account zero-point vibrational corrections. Coupled-cluster basis-set convergence is analyzed and extrapolation techniques are employed to estimate basis-set-limit quantities, thereby establishing an accurate benchmark data set. Together with the set provided for rotational g-tensors and magnetizabilities in our previous work [O. B. Lutnæs, A. M. Teale, T. Helgaker, D. J. Tozer, K. Ruud, and J. Gauss, J. Chem. Phys. **131**, 144104 (2009)], it provides a substantial source of consistently calculated high-accuracy data on second-order magnetic response properties. The utility of this benchmark data set is demonstrated by examining a wide variety of Kohn–Sham exchange–correlation functionals for the calculation of these properties. None of the existing approximate functionals provide an accuracy competitive with that provided by CCSD or CCSD(T) theory. The need for a careful consideration of vibrational effects is clearly illustrated. Finally, the pure coupled-cluster results are compared with the results of Kohn–Sham calculations constrained to give the same electronic density. Routes to future improvements are discussed in light of this comparison. © *2013 American Institute of Physics*. [http://dx.doi.org/10.1063/1.4773016]

I. INTRODUCTION

The computational simplicity and reasonable accuracy for a range of chemical applications that may be attained using Kohn–Sham density-functional theory (DFT) has led, over the previous two decades, to its current status as the most frequently applied method in computational chemistry.[1,2] In Kohn–Sham theory, an auxiliary system of non-interacting electrons with the same electron density ρ as that of the physical, interacting system is introduced. The total electronic energy is then decomposed into components that may be evaluated exactly from the non-interacting system (i.e., the non-interacting kinetic energy, the electron–nuclear attraction energy, and the classical Coulomb repulsion energy) and a remaining component, called the exchange–correlation energy, $E_{\mathrm{xc}}[\rho]$. The exact form of this functional is unknown and must be approximated. The success of Kohn–Sham theory thus rests on the availability of useful approximations to the exchange–correlation functional. Unfortunately, no systematic hierarchy of functionals that converge to the exact $E_{\mathrm{xc}}[\rho]$ exists. To assess the quality of the available approximate exchange–correlation functionals, it is therefore necessary to benchmark against accurate experimental or theoretical data for the molecular properties of interest.

By contrast, coupled-cluster theory provides a systematic path towards the exact description of the electronic system, with a well-defined hierarchy of increasingly accurate levels of theory. By truncating the cluster expansion at the level of double excitations, we obtain the coupled-cluster singles–doubles (CCSD) model,[3] which typically provides reasonable but usually not high accuracy for a range of molecular properties. For higher accuracy, triple excitations can be included in a perturbative fashion at the coupled-cluster singles–doubles–perturbative-triples [CCSD(T)] level of theory,[4] the gold standard of computational quantum chemistry, against which other methodologies are typically compared.

In the present paper, we examine the accuracy and quality of Kohn–Sham theory for nuclear-magnetic-resonance (NMR) shielding constants and spin–rotation constants by comparing Kohn–Sham results (obtained using a variety of approximate exchange–correlation functionals for a wide range of molecules) with coupled-cluster results. Where possible, the accuracy of the coupled-cluster benchmark data is established by comparison with experimental results, taking into account zero-point vibrational corrections. High-accuracy coupled-cluster studies of gas-phase shielding constants have previously been presented for ^{13}C nuclei,[5] for

^{19}F nuclei,[6] for ^{17}O nuclei,[7] and for ^{15}N and ^{31}P nuclei.[8] For an early assessment and benchmarking of Kohn–Sham shieldings, see the work of Magyarfalvi and Pulay[9] from 2003. We also note the work by Keal *et al.*[10] and the recent papers by Kupka and co-workers.[11–13]

Our benchmark data set has been compiled for a set of 28 small molecules considered previously in Ref. 14. We have restricted our benchmark set to molecules where relativistic corrections to the calculated properties are expected to be small, allowing the use of standard coupled-cluster results to determine highly accurate benchmark results. All calculations employ (rotational) London atomic orbitals (LAOs) to determine NMR shielding and spin–rotation constants in a gauge-origin independent manner.[15–19] Where possible, the calculated constants are compared with experimental values, taking into account zero-point vibrational corrections. Basis-set extrapolation[20–22] is used to estimate the coupled-cluster basis-set limit, providing a useful reference data set for benchmarking less accurate computational methods. Taken together with the data set presented by Lutnæs *et al.* for magnetizabilities and rotational *g* tensors in Ref. 14, these results provide accurate benchmark data for a range of second-order magnetic response properties.

In Sec. II, we briefly review the key theoretical aspects pertinent to the evaluation of the spectroscopic constants considered in this work and their zero-point vibrational corrections. In Sec. III, we give computational details of the calculations, including information on the basis sets and on the extrapolation techniques employed to obtain basis-set-limit quantities.

Next, in Sec. IV, we present a discussion of the available experimental data for comparison with our results and define a set of empirical equilibrium data taking account of ro-vibrational corrections. The benchmark coupled-cluster data set is presented in Sec. V, along with errors relative to these data (extensive additional information may be found in the supplementary material[23]). The importance of vibrational corrections when comparing with calculated data is highlighted and an analysis of the convergence of the results with respect to basis set and coupled-cluster excitation level is given. The utility of the benchmark set is illustrated in Sec. VI by analyzing the performance of a variety of exchange–correlation functionals. Particular attention is paid to the types of exchange–correlation functionals used and the evaluation of the orbital-dependent forms is carried out using both the conventional and optimized-effective-potential (OEP) approaches.[24,25] In Sec. VII, we compare the performance of coupled-cluster methods with DFT calculations constrained to reproduce the same coupled-cluster density, using a constrained-search technique.[26] Finally, Sec. VIII contains some concluding remarks and directions for future work.

II. THEORY

NMR shielding constants have great importance in chemistry due to the widespread use of NMR spectroscopy in structural characterization. Because of the surrounding electrons, the local field experienced by a nucleus inside a molecule in an NMR experiment differs slightly from the externally applied magnetic field. This modification of the external field is described by the NMR shielding constant, which in NMR experiments is measured relative to some chosen reference compound. To establish absolute shieldings, one may make use of the fact that spin–rotation constants (which can be accurately measured) are closely related to the paramagnetic part of the nuclear magnetic shielding tensor.[27] The spin–rotation constant of a given nucleus describes the interaction between the magnetic moment of that nucleus and the magnetic field arising from the rotational motion of the molecule. By combining measured spin–rotation tensors with accurately calculated diamagnetic contributions to the shielding tensor, absolute shielding constants may be determined. Here, we perform accurate calculations of the NMR shielding and spin–rotation tensor.

The NMR shielding tensor $\boldsymbol{\sigma}_K$ and spin–rotation tensor $\mathbf{C}_K$ are second-order magnetic properties and may be identified as the derivatives[28,29]

$$\boldsymbol{\sigma}_K = \left.\frac{\mathrm{d}^2 E}{\mathrm{d}\mathbf{B}\mathrm{d}\mathbf{M}_K}\right|_{\mathbf{B},\mathbf{M}_K=\mathbf{0}}, \tag{1}$$

$$\mathbf{C}_K = \left.\frac{\mathrm{d}^2 E}{\mathrm{d}\mathbf{J}\mathrm{d}\mathbf{I}_K}\right|_{\mathbf{J},\mathbf{I}_K=\mathbf{0}}, \tag{2}$$

where E is the electronic energy (excluding the nuclear spin–Zeeman term), $\mathbf{B}$ is the external magnetic field, $\mathbf{J}$ is the rotational angular momentum, and $\mathbf{M}_K = \gamma_K \mathbf{I}_K$ is the magnetic moment associated with nucleus K of nuclear spin $\mathbf{I}_K$ and gyromagnetic ratio γ_K. In these equations and throughout this paper, atomic units are used unless otherwise stated. It is important to note that different sign conventions exist for the spin–rotation constant. We here follow the sign convention adopted in most recent experimental papers, which differs from the convention used by Flygare and Lowe[27,30] in their classic papers.

In all of our calculations, we use LAOs, also known as gauge-including atomic orbitals (GIAOs).[31] The use of these orbitals for calculating magnetic properties involving an external magnetic field is now standard and preferable to other procedures for imposing gauge-origin independence because of its rapid basis-set convergence.[28] For rotating molecules, the rotational LAOs are defined as[17]

$$\omega_\mu(\mathbf{B},\mathbf{J},\mathbf{r}) = \mathrm{e}^{-\mathrm{i}\left(\frac{1}{2}\mathbf{B}\times(\mathbf{R}_\mu-\mathbf{R}_\mathrm{O})-\mathbf{I}^{-1}\mathbf{J}\times\mathbf{R}_\mu\right)\cdot\mathbf{r}}\chi_\mu(\mathbf{r}), \tag{3}$$

where $\chi_\mu(\mathbf{r})$ is a usual atomic basis function, $\mathbf{R}_\mathrm{O}$ is the origin of the vector potential, and $\mathbf{I}^{-1}$ is the inverse moment-of-inertia tensor. When LAOs are used, the relation between the paramagnetic contribution to the shielding tensor and the spin–rotation tensor is[17]

$$\mathbf{C}_K = 2\gamma_K\left(\boldsymbol{\sigma}_K^{\mathrm{LAO}} - \boldsymbol{\sigma}_K^{\mathrm{d}}(\mathbf{R}_K)\right)\mathbf{I}^{-1} + \mathbf{C}_K^{\mathrm{n}}, \tag{4}$$

TABLE I. Nuclei considered in the present study and their absolute shielding scales in the gas phase (ppm).

Nucleus	Ref. molecule	Value	Ref.
^{15}N	NH_3	264.54(20)	83, 84
^{1}H	H_2O	30.052(15)	85
^{19}F	HF	409.6(10)	86
^{17}O	H_2O	325.3(3)	87
^{13}C	CO	0.9(9)	86
^{33}S	OCS	817(12)[a]	88, 89
^{31}P	PH_3	587.1	90

[a]Values based on this shielding scale are excluded from the statistical analysis. See text for details.

where $\boldsymbol{\sigma}_K^{\mathrm{LAO}}$ is the shielding tensor calculated using LAOs, $\boldsymbol{\sigma}_K^{\mathrm{d}}(\mathbf{R}_K)$ is the diamagnetic contribution to the shielding tensor calculated with standard atomic orbitals and the gauge origin at $\mathbf{R}_K$ (the position of nucleus K), and $\mathbf{C}_K^{\mathrm{n}}$ is the nuclear contribution to the spin–rotation tensor.

In the present work, we utilize the implementation of LAOs in the DALTON quantum-chemistry package[32] for the restricted Hartree–Fock (RHF) and Kohn–Sham calculations and the implementation of LAOs in the Mainz–Austin–Budapest version of the ACESII package[33] for the coupled-cluster calculations.

III. COMPUTATIONAL DETAILS

The NMR shielding and spin–rotation constants were calculated and analyzed following the same procedure as for the magnetizabilities and rotational g tensors in Ref. 14, on the same set of 28 molecules, chosen to provide a varied and challenging benchmark set amenable to a coupled-cluster treatment in large basis sets—see Tables I and II, respectively, for the nuclei and molecules considered in this study. All shielding and spin–rotation constants were calculated at the geometry optimized at the all-electron CCSD(T)/cc-pVTZ level of theory and are available in the supplementary material.[23] A range of standard spherical-harmonic AO basis sets from Dunning's correlation-consistent basis-set families were chosen:[34–37] cc-pVXZ, cc-pCVXZ, aug-cc-pVXZ, and aug-cc-pCVXZ with $2 \leq X \leq 4$. In the coupled-cluster calculations, all electrons were correlated.

To establish the benchmark data set, Hartree–Fock, CCSD, and CCSD(T) calculations were carried out with each basis set. To estimate the Hartree–Fock basis-set-limit property $P_{\mathrm{HF},\infty}$, we use the extrapolation formula[21]

$$P_{\mathrm{HF},\infty} = \frac{P_{\mathrm{HF},X}\exp(\alpha X) - P_{\mathrm{HF},Y}\exp(\alpha Y)}{\exp(\alpha X) - \exp(\alpha Y)} \qquad (5)$$

with $\alpha = 1.63$, where $P_{\mathrm{HF},X}$ is the property calculated at the Hartree–Fock level with a basis of cardinal number X. The final correlated basis-set limit result P_∞ is then obtained by adding a two-point extrapolated correlation contribution in the manner[20,21]

$$P_\infty = P_{\mathrm{HF},\infty} + \frac{X^3 P_{\mathrm{corr},X} - Y^3 P_{\mathrm{corr},Y}}{X^3 - Y^3}, \qquad (6)$$

where $P_{\mathrm{corr},X}$ is the correlation contribution to the property calculated with cardinal number X. In all extrapolations, we used cardinal numbers $X = 4$ and $Y = 3$.

The formulae described above have been developed for extrapolations of Hartree–Fock and correlation energies, respectively. Apart from applications to total energies, they have been very successful for extrapolation of atomization energies and reaction enthalpies. Their use for the direct extrapolation of molecular properties is less well founded and less used. We here mention applications to dipole moments,[38] spectroscopic constants,[39] and to molecular gradients.[40] For molecular forces, in particular, the use of energy-based extrapolation schemes is justified by the observation that force extrapolation is equivalent to force evaluation of extrapolated potential energy surfaces. Extrapolated properties other than the energy—for instance, extrapolated shielding constants—may be used to estimate uncertainties related to basis-set incompleteness.

These extrapolated coupled-cluster results constitute an accurate benchmark set of data, against which we compare Kohn–Sham results obtained using a range of exchange–correlation functionals in the following four categories: the local-density approximation (LDA);[41,42] the generalized-gradient approximation (GGA) with the functionals BLYP,[43,44] PBE,[45] and KT2;[46] hybrid Kohn–Sham theory with the functionals B3LYP,[47,48] B97-2,[49] B97-3,[50] and PBE0;[51] and range-separated hybrid Kohn–Sham theory as represented by the CAM-B3LYP functional.[52]

In addition, for the orbital-dependent forms in the latter two categories, we have applied the OEP method to adhere strictly to the Kohn–Sham framework. A number of previous studies have shown consistent improvements in magnetic properties when multiplicative potentials are employed.[53–63] In the present work, we use the OEP algorithm of Yang and Wu,[64,65] which has been implemented in a development version of the DALTON quantum-chemistry code. Specifically, we use an approximate Newton method with a truncated-singular-value-decomposition (TSVD) cut-off of 10^{-6} on the eigenvalues of the approximate Hessian and a convergence tolerance of 10^{-6} on the gradient norm. In common with other codes, our OEP code has the functionality to use a separate, auxiliary basis for the expansion of the Kohn–Sham potential $v_{\mathrm{KS}}(\mathbf{r})$, different from the primary orbital basis. However, in all calculations presented here, the same basis is used for the orbitals and potentials, thereby ensuring smooth potentials. For discussion of the issues surrounding basis-set choices in OEP calculations, see Refs. 66–77. To ensure that our basis is adequate for the purposes of the present work, we have performed OEP calculations for the LDA and GGA functionals in each of the basis sets considered. For these local, orbital-independent exchange–correlation functionals, the results obtained using OEPs should be identical to those obtained from a conventional evaluation, since their potentials are already multiplicative. In practice, we obtain mean and mean absolute relative deviations agreeing to better than 0.7% in the largest basis set considered.

To examine the connection between the coupled-cluster and Kohn–Sham theories further, we have performed Kohn–Sham calculations of NMR shielding and spin–rotation

TABLE II. Absolute calculated and experimental isotropic shielding constants (ppm). The calculated shieldings have been obtained using the RHF, CCSD, and CCSD(T) models in the aug-cc-pCVQZ basis with all electrons correlated; the extrapolated aug-cc-pCV[TQ]Z results have been obtained as described in the text. Vibrational corrections have been evaluated using B3LYP/aug-cc-pCVTZ theory. Experimental and empirical equilibrium data contained in parentheses are excluded from the statistical analysis, see text for further details.

Molecule	Nucleus	RHF	CCSD	CCSD(T)	Extrap.	Exp.[a]	Vib.	Emp. Eq.[b]	Exp. Ref.	Exp. Notes[c]
HF	^{1}H	28.25	28.89	28.96	28.83	28.51	− 0.33	28.84	85, 93	Gas 298 K
	^{19}F	414.68	419.69	420.17	420.31	409.6	− 11.80	421.40	86, 96	SR 300 K
CO	^{17}O	− 89.41	− 56.82	− 53.63	− 55.05	− 62.74	− 5.75	− 56.99	94, 97	SR 300 K
	^{13}C	− 26.63	− 0.95	4.03	2.24	0.9	− 2.42	3.32	86, 98	SR 300 K
N_2	^{15}N	− 113.20	− 64.70	− 58.76	− 60.43	− 61.6	− 4.33	− 57.27	83	Gas 300 K
H_2O	^{17}O	328.13	337.02	337.97	338.01	323.6	− 14.23	337.83	94, 95	Gas 300 K
	^{1}H	30.59	30.75	30.77	30.65	30.05	− 0.52	30.57	85	Gas 298 K
HCN	^{15}N	− 51.13	− 16.92	− 12.72	− 14.11	− 20.4	− 10.24	− 10.24	83	Gas 300 K
	^{13}C	70.56	83.44	85.71	84.58	82.0	− 2.44	84.44	92	Gas 300 K
	^{1}H	29.24	29.12	29.04	29.01	27.78	− 0.76	28.54	99, 85	Gas 393 K
HOF	^{17}O	− 135.97	− 65.46	− 66.07	− 68.92		− 32.52			
	^{1}H	19.09	19.91	19.72	19.57	18.511	− 0.74	19.25	100	Gas 295 K
	^{19}F	288.90	205.00	193.01	192.21	169.6	− 15.87	185.47	100	Liquid 193 K
O_3	$^{17}O_{mid}$	− 2706.37	− 990.62	− 763.52	− 763.70	(−743[d])	− 40.64	(− 702.36)	101	Solution
	$^{17}O_{term}$	− 2775.57	− 1411.38	− 1215.81	− 1221.62	(−1309[d])	− 89.13	(− 1219.87)	101	Solution
NH_3	^{15}N	262.57	269.85	270.79	270.66	264.54	− 8.71	273.25	83	Gas 300 K
	^{1}H	31.65	31.54	31.52	31.44	30.68	− 0.61	31.29	85	Gas 298 K
H_2CO	^{1}H	22.51	22.21	22.02	21.99	18.3	− 0.51[e]	18.81[e]	84	SR
(formaldehyde)	^{17}O	− 441.56	− 380.37	− 376.45	− 378.61	(−427)	− 16.28[e]	(− 410.72[e])	102, 103	SR
	^{13}C	− 7.87	2.03	3.36	1.53	− 0.5	− 4.21[e]	3.71[e]	102, 104	SR
CH_4	^{13}C	194.98	198.81	199.25	198.93	195.0	− 3.74	198.74	92	Gas 300 K
	^{1}H	31.58	31.38	31.35	31.30	30.61	− 0.63	31.24	85, 105	Gas 298 K
C_2H_4	^{13}C	59.51	69.19	70.83	69.71	64.4	− 5.34	69.74	92	Gas 300 K
	^{1}H	26.22	26.16	26.10	26.05	25.43	− 0.53	25.96	99	Gas 295 K
AlF	^{27}Al	580.18	575.60	573.66	572.89		0.45			
	^{19}F	228.98	222.02	212.52	211.85		− 2.13			
CH_3F	^{19}F	486.68	483.65	482.66	482.88	470.6	− 12.85	483.45	106	Gas 300 K
	^{13}C	125.02	123.71	122.96	122.15	116.7	− 5.13	121.83	92	Gas 300 K
	^{1}H	27.93	27.51	27.40	27.35	26.6	− 0.63	27.23	107	Gas 295 K
C_3H_4	$^{13}C_3$	193.28	192.97	192.61	192.10	190.4	− 5.51	195.91	108, 109	Liquid
(cyclopropene)	$^{13}C_1$	70.75	83.06	84.72	83.69	84	− 6.56	90.56	108, 109	Liquid
	$^{1}H_1$	24.10	24.46	24.42	24.37	24.0	− 0.50	24.50	110, 109	Liquid
	$^{1}H_3$	30.95	30.77	30.70	30.64	30.1	− 0.69	30.79	110, 109	Liquid
FCCH	^{19}F	428.27	426.42	423.70	423.55	(446.05)	− 15.36	(461.41)	111, 112	Not reported
	$^{13}C_H$	176.47	179.47	180.58	179.86	168.9	− 5.30	174.20	113, 114	Liquid
	$^{13}C_F$	100.82	101.45	100.86	100.06	93.9	− 5.27	99.17	113, 114	Liquid
	^{1}H	30.55	30.55	30.54	30.49	(31.9)	− 1.00	(32.9)	111	Not reported
FCN	^{19}F	377.67	378.24	374.31	374.10	(344.70)	− 7.63	(352.33)	113, 115	Liquid
	^{14}N	91.84	114.64	119.24	117.89		− 8.00			
	^{13}C	75.26	82.16	83.27	82.24		− 1.44			
H_2S	^{33}S	711.31	736.01	739.98	739.05	(707.1)	− 26.78	(733.88)	88	Liquid
	^{1}H	30.56	30.56	30.55	30.45	30.53	− 0.41	30.94	99	Gas 295 K
HCP	^{13}C	13.31	34.51	38.87	37.55	32.97	− 4.35	37.32	116	Liquid
	^{1}H	30.13	29.73	29.59	29.56		− 0.93			
	^{31}P	339.69	379.94	390.77	388.04	353.05	− 22.91	375.96	116	Liquid
HFCO	^{1}H	24.41	24.04	23.90	23.86		− 0.48			
	^{19}F	187.85	175.71	165.82	165.27	147.7	− 12.32	160.02	117	Liquid
	^{13}C	33.43	39.67	40.98	39.63		− 2.43			
	^{17}O	− 129.55	− 99.30	− 92.60	− 94.33		− 13.20			
H_2C_2O	^{1}H	29.39	29.31	29.27	29.19	31.29	− 0.40	31.69	118	Liquid 211 K
(ketene)	$^{13}C_H$	189.32	192.81	193.93	193.32	184.5	− 2.91	187.41	119	Liquid 213 K
	$^{13}C_O$	− 14.87	− 6.26	− 4.76	− 6.34	− 7.0	− 2.32	− 4.68	119	Liquid 213 K
	^{17}O	− 27.40	− 9.50	− 4.89	− 5.92		− 4.95			
LiF	^{7}Li	90.55	89.67	89.46	89.34	87.5	0.09[e]	87.41[e]	120, 121	SR
	^{19}F	390.83	385.88	382.80	382.48	374.3	1.14[e]	373.16[e]	120, 121	SR
LiH	^{7}Li	89.55	89.51	89.49	89.32	90.6	0.13[e]	90.47[e]	120, 122	SR
	^{1}H	26.59	26.58	26.57	26.58	25.7	− 0.10[e]	25.80[e]	120, 122	SR

TABLE II. (*Continued*)

Molecule	Nucleus	RHF	CCSD	CCSD(T)	Extrap.	Exp.[a]	Vib.	Emp. Eq.[b]	Exp. Ref.	Exp. Notes[c]
N_2O	$^{15}N_{end}$	62.73	99.79	107.66	106.45	99.5	− 8.41	107.91	83	Gas 300 K
	$^{15}N_{cent}$	− 33.42	5.24	13.62	12.56	11.3	− 3.91	15.21	83	Gas 300 K
	^{17}O	174.80	199.10	200.00	199.02	178.3	− 12.94	191.24	94, 95	Gas 300 K
OCS	^{17}O	76.61	95.12	97.76	96.76	85.5	− 7.92	93.42	123	Gas 300 K
	^{33}S	787.59	797.33	798.70	796.69	(817)	− 17.28	(834.28)	124	Gas 323 K
	^{13}C	7.33	25.05	31.43	30.18	30	− 2.13	32.13	92	Gas 300 K
OF_2	^{17}O	− 443.82	− 414.60	− 442.10	− 447.09	− 495.3	− 44.29	− 451.01	95	Gas 300 K
	^{19}F	22.38	− 7.52	− 21.98	− 23.95	− 60.3	− 25.02	− 35.28	125	Liquid
H_4C_2O	^{17}O	378.82	366.37	363.77	363.23	336.5	− 18.43	354.93	126	Liquid
(oxirane)	^{13}C	155.44	154.57	153.94	153.20	147.9	− 5.41	153.31	127	Liquid
	^{1}H	29.73	29.30	29.19	29.14	30.95	− 0.65	31.60	128	Liquid
PN	^{31}P	− 108.45	29.83	55.65	50.59	53	− 6.91[e]	59.91[e]	113, 129	SR
	^{14}N	− 506.50	− 362.29	− 341.44	− 343.97	− 349	− 5.34[e]	− 343.66[e]	113, 129	SR
SO_2	^{17}O	− 335.59	− 247.08	− 240.32	− 242.68	(− 231.0)	− 16.46	(− 214.54)	130	Gas 300 K
	^{33}S	− 395.22	− 232.85	− 195.38	− 203.45	(− 152.5)	− 12.90	(− 139.60)	130	Gas 333 K

[a]Relative to absolute shielding scales of Table I. The liquid data have been related to this scale by the use of $\sigma(C)^{liquid}_{TMS} = 186.97$ ppm,[86,91] $\sigma(C)^{liquid}_{benzene} - \sigma(C)^{liquid}_{TMS} = -128.1$ ppm,[92] $\sigma(H)^{liquid}_{TMS} = 33.485$ ppm,[85,91] $\sigma(F)^{liquid}_{CFCl_3} = 188.3$ ppm,[86,93] $\sigma(O)^{liquid}_{H_2O} = 287.5$ ppm,[94] $\sigma(H)^{gas}_{CH_4} = 30.61$ ppm,[85] and $\sigma(H)^{liquid}_{H_2O} = 35.790$ ppm.[85]

[b]Empirical equilibrium values obtained by subtracting the ro-vibrational contribution from the experimental value.

[c]SR indicates that the shielding consists of a paramagnetic contribution from the experimentally determined spin–rotation constants and a theoretical value for the diamagnetic contribution.

[d]The gas–liquid shift of 36.1 ppm from Ref. 95 has been accounted for.

[e]At $T = 0$ K.

constants where the density is constrained to be that of coupled-cluster theory, obtained using the Lagrangian approach of Helgaker and Jørgensen.[78–80] To perform these constrained Kohn–Sham calculations, we have adopted the constrained-search approach of Wu and Yang[81] (similar to the OEP algorithm above), denoting the results based on CCSD and CCSD(T) densities by KS[CCSD] and KS[CCSD(T)], respectively. For these calculations, we follow the same approach as for the OEP calculations, expanding the effective potential and the orbitals in the same basis, with a TSVD cutoff of 10^{-6} on the Hessian eigenvalues and a convergence tolerance of 10^{-6} on the gradient norm. For further details, see Ref. 81. The coupled-cluster property calculations were performed using the Mainz–Austin–Budapest version of ACESII.[33] All remaining calculations were performed with a development version of DALTON.[32] The ro-vibrational corrections have been calculated at the DFT B3LYP/aug-cc-pCVTZ level using DALTON based on perturbation theory as described in Ref. 82. The accuracy of the obtained corrections has been confirmed by ensuring that similar corrections are obtained with other exchange–correlation functionals.

IV. EXPERIMENTAL AND EMPIRICAL EQUILIBRIUM DATA

Good quality experimental data are available for both NMR shielding constants and spin–rotation constants. Where possible, we compare calculated results with gas-phase experimental results and empirical equilibrium values, obtained from experimental values by subtracting calculated vibrational contributions. The nuclei for which NMR shielding constants and spin–rotation tensors are studied are listed in Table I.

A. NMR shielding constants

In Table II, experimental shielding-constant values are collected from the literature. These values have been determined in two different ways. In one approach, the spin–rotation constant is used to determine the paramagnetic contribution to the shielding constant using Eq. (4), while the diamagnetic contribution is determined theoretically. In this approach, the main source of error is usually the uncertainty in the spin–rotation constant since the diamagnetic contribution is only dependent on the ground-state wave function and can be obtained accurately by quantum-chemical calculations. The shieldings obtained in this manner from spin–rotation constants are labeled "SR" in Table II.

The other way the experimental data have been determined is via NMR chemical shifts measured relative to the shielding of a reference molecule. The error is then almost entirely determined by the error in the value of the absolute shielding constant of the reference, which has normally been obtained as described above. The experimental data based on measured NMR shifts are labeled "gas" or "liquid" in Table II, depending on whether the experiment was performed in the gas or liquid phase, respectively. When necessary, the values taken from the literature have been adjusted to conform to the absolute shielding scales listed in Table I. If the values quoted in this table are updated in the future, the shielding constants obtained from shift experiments in Table II should be updated accordingly.

The values in Table I have been collected as described below. For hydrogen, the value of 30.052 ppm for the shielding of water reported by Raynes[85] is used. This value is based on NMR experiments carried out for liquid water by Phillips *et al.*[131] and was corrected by Raynes[85] for gas–liquid effects. In the case of ^{19}F, we use the shielding scale suggested by

Sundholm *et al.*[86] It has been derived from the fluorine spin–rotation constant for HF[96] using accurately computed values for the diamagnetic part and the required ro-vibrational corrections. For ^{17}O, we rely on the recently determined shielding scale by Puzzarini *et al.*[87] based on measurements of the spin–rotation constants for $H_2{}^{17}O$ using high-resolution rotational spectroscopy. It differs slightly from an older scale of Wasylishen and Bryce[94] based on the spin–rotation constant for $C^{17}O$ and which can be considered less accurate.[87] The carbon shielding scale is derived from the spin–rotation constant determined for ^{13}CO in Ref. 98. The quoted value of 0.9(9) ppm for the shielding in CO has been derived in Ref. 86 using values from high-level quantum-chemical calculations for the diamagnetic contribution and the ro-vibrational corrections. The nitrogen shielding scale is based on the experimental value of the spin–rotation constant for $^{14}NH_3$ reported in Ref. 84. The conversion of the spin–rotation constant to the nitrogen shielding value of $^{15}NH_3$ was carried out in Ref. 83. In the case of ^{33}S, the reference value for the shielding scale is the shielding determined for OCS[89,124] based on the measured spin–rotation constant[132] and high-level quantum-chemical calculations for the diamagnetic contribution and ro-vibrational corrections. Finally, the currently available ^{31}P scale has been established in Ref. 90 and is based on the experimental spin–rotation constant for PH_3[133] and the ro-vibrational corrections given in Ref. 90.

To obtain empirical equilibrium shielding constants that correspond to a non-vibrating and non-rotating molecule at the equilibrium geometry, ro-vibrational contributions have been calculated (at 0 K or 300 K, for the same isotopologues as in experiment) and then subtracted from the experimental values. The resulting ro-vibrational corrections and empirical equilibrium shieldings are also listed in Table II. When the experimental value has been determined in the gas phase, the empirical equilibrium shieldings are directly comparable with the calculated shieldings at the equilibrium geometry. In case of liquid-phase values, medium effects should in principle be accounted for but this has not been done in the present work.

We note that, for the shielding constants, the largest contribution to the ro-vibrational correction is the zero-point vibrational contribution—temperature effects are much smaller, rarely exceeding 10% of the total ro-vibrational correction. The variation in the ro-vibrational contribution among isotopologues is also very small, usually on the order of 10^{-2} ppm.

For the comparison with experiment, essential to establish the high accuracy of the CCSD(T) calculations, some experimental data points were excluded from the statistical analysis. These include all ^{33}S shieldings, as the corresponding scale is based on a rather inaccurate shielding value for OCS, determined from the measured spin–rotation constant without a proper treatment of ro-vibrational effects. In addition, the ^{17}O shielding of formaldehyde, also determined from spin–rotation data, has error bars that are too large for the value to be included in the statistical analysis. Furthermore, the ^{19}F and ^{1}H values for FCCH, the ^{19}F shielding of FCN, and the ^{17}O shieldings of SO_2 are of limited accuracy and have therefore been excluded from the statistical analysis. These data have been included in Table II in parentheses, to indicate that they are not included in the statistical analysis in the present work.

B. Spin–rotation constants

For spin–rotation constants, we consider 149 tensor elements for the 28 molecules in Table III, which collects the experimental data for the spin–rotation constants included in this study. Overall, experimental values for a total of 57 tensor elements are available with sufficient accuracy for comparison with the calculated values. A further 13 experimental values are included in Table III in parentheses, for which the experimental determination is not sufficiently precise to allow meaningful discrimination between the computational methods considered. Since the values of spin–rotation constants depend explicitly on the nuclear mass, we have matched our calculated values to the specific isotopologues used in the experimental determinations.

The values quoted have been obtained in the gas phase either by means of molecular-beam experiments or via the analysis of the hyperfine structure in the corresponding rotational spectra. Consequently, they can be identified roughly with the values for the isolated molecules. These values include zero-point vibrational effects but no temperature effects since they result from an analysis of individual ro-vibrational states.

A rigorous comparison of theoretical and experimental values should thus account for zero-point vibrational corrections. These have been calculated in the same way as for the shielding constants (using the procedure described in Ref. 82) and subtracted from the experimental values, resulting in the empirical equilibrium values reported in Table III. However, it should be noted that this perturbative treatment of vibrational effects fails for polyatomic linear molecules because of numerical instabilities associated with the bending modes. For HCN, FCCH, and HCP, therefore, no vibrational corrections have been calculated.

V. BENCHMARKING COUPLED-CLUSTER THEORY

In the present section, we examine the performance of the *ab initio* Hartree–Fock and coupled-cluster models by comparing the shielding and spin–rotation constants calculated using these models with the empirical equilibrium values in Tables II and III, respectively.

A. NMR shielding constants

Table IV contains the mean errors (MEs), the mean absolute errors (MAEs), the maximum absolute errors (MxAEs), the mean relative errors (MREs), the mean absolute relative errors (MAREs) and the standard deviations (SDs) of the RHF, CCSD, and CCSD(T) shielding constants relative to the empirical equilibrium values in Table II for the basis sets cc-pV*X*Z, cc-pCV*X*Z, aug-cc-pV*X*Z, and aug-cc-pCV*X*Z, with $2 \leq X \leq 4$. The error measures are presented for all molecules except O_3, whose multi-reference nature presents a substantial challenge for single-reference quantum-chemical approaches (errors that include the ozone shieldings

TABLE III. Calculated and experimental spin–rotation constants (kHz). The calculated spin–rotation constants have been obtained using the RHF, CCSD, and CCSD(T) models in the aug-cc-pCVQZ basis with all electrons correlated; the extrapolated aug-cc-pCV[TQ]Z results have been obtained as described in the text. Vibrational corrections have been evaluated using B3LYP/aug-cc-pCVTZ theory. Experimental and empirical equilibrium values in parentheses are excluded from the statistical analysis, see text for details.

Molecule	Isotopologue	Nucleus	Tensor element	RHF	CCSD	CCSD(T)	Extrap.	Exp.	Vib.	Emp. Eq.	Exp. Ref.
HF	$^{1}H^{19}F$	^{1}H	$C_{aa} = C_{bb}, C_{cc} = 0$	− 68.56	− 72.20	− 72.74	− 71.95	− 71.10	0.65	−71.75	96
	$^{1}H^{19}F$	^{19}F	$C_{aa} = C_{bb}, C_{cc} = 0$	309.65	282.97	280.08	279.86	307.65	28.26	279.39	96
CO	$^{13}C^{16}O$	^{13}C	$C_{aa} = C_{bb}, C_{cc} = 0$	36.13	32.99	32.37	32.61	32.70	0.02	32.68	98
	$^{12}C^{17}O$	^{17}O	$C_{aa} = C_{bb}, C_{cc} = 0$	− 33.58	− 31.34	− 31.11	− 31.22	− 31.609	− 0.10	−31.51	97
N_2	$^{15}N^{15}N$	^{15}N		− 22.52	− 19.40	− 19.10	− 19.18	(− 22)	− 0.05	(−22.05)	134
H_2O	$^{1}H^{1}H^{16}O$	^{1}H	C_{aa}	− 34.87	− 35.66	− 35.91	− 35.54	− 35.05	1.23	−36.28	135
	$^{1}H^{1}H^{16}O$	^{1}H	C_{bb}	− 31.73	− 32.27	− 32.35	− 32.02	− 31.02	0.63	−31.65	135
	$^{1}H^{1}H^{16}O$	^{1}H	C_{cc}	− 33.72	− 34.46	− 34.59	− 34.26	− 32.99	1.45	−34.44	135
	$^{1}H^{1}H^{17}O$	^{17}O	C_{aa}	− 25.08	− 21.92	− 21.77	− 21.72	− 28.477			87
	$^{1}H^{1}H^{17}O$	^{17}O	C_{bb}	− 31.02	− 26.22	− 25.53	− 25.60	− 28.504			87
	$^{1}H^{1}H^{17}O$	^{17}O	C_{cc}	− 19.23	− 17.40	− 17.20	− 17.21	− 18.382			87
HCN	$^{1}H^{12}C^{14}N$	^{1}H	$C_{aa} = C_{bb}, C_{cc} = 0$	− 4.92	− 4.78	− 4.75	− 4.73	− 4.35			136
	$^{1}H^{13}C^{14}N$	^{13}C	$C_{aa} = C_{bb}, C_{cc} = 0$	18.85	17.64	17.42	17.54	17.50			137
	$^{1}H^{12}C^{14}N$	^{14}N	$C_{aa} = C_{bb}, C_{cc} = 0$	11.02	10.04	9.91	9.95	10.13			136
HOF	$^{1}H^{16}O^{19}F$	^{1}H	C_{aa}	− 65.22	− 67.08	− 67.54	− 66.83		0.91		
	$^{1}H^{16}O^{19}F$	^{1}H	C_{bb}	4.87	4.52	4.62	4.64				
	$^{1}H^{16}O^{19}F$	^{1}H	C_{cc}	− 2.98	− 2.88	− 2.87	− 2.85				
	$^{1}H^{17}O^{19}F$	^{17}O	C_{aa}	− 34.38	− 32.03	− 31.98	− 31.96		0.90		
	$^{1}H^{17}O^{19}F$	^{17}O	C_{bb}	− 22.23	− 18.98	− 19.02	− 19.15				
	$^{1}H^{17}O^{19}F$	^{17}O	C_{cc}	− 10.21	− 9.07	− 9.08	− 9.14				
	$^{1}H^{16}O^{19}F$	^{19}F	C_{aa}	9.71	17.41	17.48	17.75		3.11		
	$^{1}H^{16}O^{19}F$	^{19}F	C_{bb}	24.31	47.30	50.14	50.27				
	$^{1}H^{16}O^{19}F$	^{19}F	C_{cc}	57.21	72.11	74.70	74.95				
O_3	$^{16}O^{17}O^{16}O$	$^{17}O_{mid}$	C_{aa}	− 550.87	− 228.43	− 186.25	− 186.40	− 174.01	− 9.01	−165.00	138
	$^{16}O^{17}O^{16}O$	$^{17}O_{mid}$	C_{bb}	− 28.62	− 13.70	− 11.10	− 11.08	− 7.90	− 0.16	−7.74	138
	$^{16}O^{17}O^{16}O$	$^{17}O_{mid}$	C_{cc}	− 2.42	− 3.14	− 3.43	− 3.45	− 1.44	− 0.01	−1.43	138
	$^{17}O^{16}O^{16}O$	$^{17}O_{term}$	C_{aa}	− 501.34	− 259.12	− 231.18	− 232.02	− 269			138
	$^{17}O^{16}O^{16}O$	$^{17}O_{term}$	C_{bb}	− 35.37	− 20.81	− 18.04	− 18.10	− 18.87			138
	$^{17}O^{16}O^{16}O$	$^{17}O_{term}$	C_{cc}	− 4.96	− 4.77	− 4.72	− 4.74	− 5.08			138
NH_3	$^{14}N^{1}H$	^{14}N	$(C_{aa} + C_{bb})/2$	7.08	6.06	5.91	5.94	6.764	0.98	5.784	84
	$^{14}N^{1}H$	^{14}N	C_{cc}	7.02	6.62	6.57	6.59	6.695	0.07	6.625	84
	$^{14}N^{1}H$	^{1}H	$(C_{aa} + C_{bb})/2$	− 18.99	− 18.98	− 19.02	− 18.86	− 17.73	1.01	−18.74	84
	$^{14}N^{1}H$	^{1}H	C_{aa}	− 33.41	− 33.23	− 33.26	− 32.97				84
	$^{14}N^{1}H$	^{1}H	C_{bb}	− 4.57	− 4.74	− 4.78	− 4.76				84
	$^{14}N^{1}H$	^{1}H	C_{cc}	− 20.02	− 19.98	− 20.01	− 19.87	− 19.05	1.12	20.17	84
H_2CO	$^{1}H^{1}H^{12}C^{16}O$	^{1}H	C_{aa}	− 8.77	− 7.18	− 6.54	− 6.50	− 3.712	1.55	−5.26	139
	$^{1}H^{1}H^{12}C^{16}O$	^{1}H	C_{bb}	2.17	1.98	1.97	1.98	2.092	− 0.05	2.15	139
	$^{1}H^{1}H^{12}C^{16}O$	^{1}H	C_{cc}	− 3.01	− 2.70	− 2.65	− 2.64	− 2.408	0.20	−2.61	139
	$^{1}H^{1}H^{13}C^{16}O$	^{13}C	C_{aa}	128.25	130.81	131.11	132.43	127.86	0.27	127.59	104
	$^{1}H^{1}H^{13}C^{16}O$	^{13}C	C_{bb}	21.76	19.96	19.60	19.71	19.99	− 0.15	20.14	104
	$^{1}H^{1}H^{13}C^{16}O$	^{13}C	C_{cc}	6.94	7.03	7.12	7.16	7.61	− 0.12	7.73	104
	$^{1}H^{1}H^{12}C^{17}O$	^{17}O	C_{aa}	− 379.26	− 367.10	− 367.45	− 368.65	(− 371)	− 1.88	(−369.12)	30
	$^{1}H^{1}H^{12}C^{17}O$	^{17}O	C_{bb}	− 29.95	− 26.96	− 26.51	− 26.58	(− 25)	0.41	(−25.41)	30
	$^{1}H^{1}H^{12}C^{17}O$	^{17}O	C_{cc}	1.12	1.05	1.02	1.03	(− 2)	0.36	(−2.36)	30
CH_4	$^{1}H^{12}C$	^{1}H	C_{aa}	− 17.71	− 17.43	− 17.43	− 17.34				140
	$^{1}H^{12}C$	^{1}H	C_{bb}	− 4.68	− 4.74	− 4.75	− 4.72				140
	$^{1}H^{12}C$	^{1}H	C_{cc}	− 11.19	− 11.09	− 11.09	− 11.03	− 10.372	0.70		140
	$^{1}H^{13}C$	^{13}C	$C_{aa} = C_{bb} = C_{cc}$	16.33	15.55	15.45	15.54	15.94	0.25	15.69	92
C_2H_4	$^{1}H^{12}C^{12}C$	^{1}H	C_{aa}	− 8.65	− 8.19	− 8.08	− 8.04		0.30		
	$^{1}H^{12}C^{12}C$	^{1}H	C_{bb}	1.54	1.40	1.39	1.40				
	$^{1}H^{12}C^{12}C$	^{1}H	C_{cc}	− 2.79	− 2.74	− 2.73	− 2.72				
	$^{1}H^{13}C^{12}C$	^{13}C	C_{aa}	42.81	42.79	42.90	43.24		0.15		
	$^{1}H^{13}C^{12}C$	^{13}C	C_{bb}	15.43	14.19	13.94	14.02				
	$^{1}H^{13}C^{12}C$	^{13}C	C_{cc}	2.83	2.81	2.82	2.83				
AlF	$^{19}F^{27}Al$	^{27}Al	$C_{aa} = C_{bb}, C_{cc} = 0$	8.06	8.25	8.32	8.36		− 0.04		
	$^{19}F^{27}Al$	^{19}F	$C_{aa} = C_{bb}, C_{cc} = 0$	33.86	34.82	36.12	36.23		− 0.01		

TABLE III. (*Continued.*)

Molecule	Isotopologue	Nucleus	Tensor element	RHF	CCSD	CCSD(T)	Extrap.	Exp.	Vib.	Emp. Eq.	Exp. Ref.
CH_3F	$^{12}C^{1}H^{19}F$	^{1}H	$(C_{aa}+C_{bb})/2$	−0.65	−0.56	−0.55	−0.54	−0.8			141
	$^{12}C^{1}H^{19}F$	^{1}H	C_{aa}	0.34	0.40	0.42	0.43				141
	$^{12}C^{1}H^{19}F$	^{1}H	C_{bb}	−1.64	−1.53	−1.51	−1.51				141
	$^{12}C^{1}H^{19}F$	^{1}H	C_{cc}	−16.07	−16.23	−16.22	−16.14	−14.66			141
	$^{12}C^{1}H^{19}F$	^{19}F	$C_{aa}=C_{bb}$	−6.85	−6.39	−6.32	−6.34	−4.0			141
	$^{12}C^{1}H^{19}F$	^{19}F	C_{cc}	44.93	48.83	50.44	50.43	51.1			141
	$^{13}C^{1}H^{19}F$	^{13}C	$C_{aa}=C_{bb}$	6.28	6.45	6.50	6.54				
	$^{13}C^{1}H^{19}F$	^{13}C	C_{cc}	19.24	18.52	18.47	18.58				
C_3H_4	$^{1}H^{12}C$	$^{1}H_1$	C_{aa}	−0.75	−0.94	−0.96	−0.95				
	$^{1}H^{12}C$	$^{1}H_1$	C_{bb}	0.88	0.86	0.89	0.89				
	$^{1}H^{12}C$	$^{1}H_1$	C_{cc}	−1.51	−1.50	−1.50	−1.49				
	$^{1}H^{12}C$	$^{1}H_3$	C_{aa}	−1.54	−1.56	−1.56	−1.55				
	$^{1}H^{12}C$	$^{1}H_3$	C_{bb}	−2.27	−2.26	−2.26	−2.25				
	$^{1}H^{12}C$	$^{1}H_3$	C_{cc}	−0.56	−0.54	−0.54	−0.53				
	$^{1}H^{13}C^{12}C$	$^{13}C_1$	C_{aa}	5.60	5.47	5.47	5.51				
	$^{1}H^{13}C^{12}C$	$^{13}C_1$	C_{bb}	3.03	3.09	3.10	3.12				
	$^{1}H^{13}C^{12}C$	$^{13}C_1$	C_{cc}	−0.21	−0.11	−0.09	−0.09				
	$^{1}H^{13}C^{12}C$	$^{13}C_3$	C_{aa}	15.65	13.93	13.63	13.70				
	$^{1}H^{13}C^{12}C$	$^{13}C_3$	C_{bb}	5.74	5.79	5.83	5.86				
	$^{1}H^{13}C^{12}C$	$^{13}C_3$	C_{cc}	1.09	1.16	1.17	1.18				
FCCH	$^{19}F^{12}C^{12}C^{1}H$	^{1}H	$C_{aa}=C_{bb}, C_{cc}=0$	−1.10	−1.09	−1.09	−1.08	−0.6			142
	$^{19}F^{12}C^{12}C^{1}H$	^{19}F	$C_{aa}=C_{bb}, C_{cc}=0$	3.52	3.68	3.90	3.92	4.4			142
	$^{19}F^{13}C^{12}C^{1}H$	$^{13}C_f$	$C_{aa}=C_{bb}, C_{cc}=0$	3.53	3.54	3.55	3.57				
	$^{19}F^{12}C^{13}C^{1}H$	$^{13}C_h$	$C_{aa}=C_{bb}, C_{cc}=0$	1.82	1.77	1.75	1.77				
FCN	$^{19}F^{12}C^{14}N$	^{19}F	$C_{aa}=C_{bb}, C_{cc}=0$	8.32	8.29	8.64	8.66				
	$^{19}F^{12}C^{14}N$	^{14}N	$C_{aa}=C_{bb}, C_{cc}=0$	1.62	1.47	1.44	1.45				
	$^{19}F^{13}C^{14}N$	^{13}C	$C_{aa}=C_{bb}, C_{cc}=0$	4.44	4.29	4.27	4.29				
H_2S	$^{1}H^{32}S$	^{1}H	C_{aa}	−17.59	−17.77	−17.84	−17.71	−16.062[a]	0.47	−16.53	143
	$^{1}H^{32}S$	^{1}H	C_{bb}	−13.50	−13.72	−13.78	−13.65				143
	$^{1}H^{32}S$	^{1}H	C_{cc}	−17.51	−17.33	−17.34	−17.23				143
	$^{1}H^{33}S$	^{33}S	C_{aa}	18.84	18.62	18.56	18.61	(8.4)	3.45	(4.95)	144
	$^{1}H^{33}S$	^{33}S	C_{bb}	64.06	57.36	56.31	56.52	(52)	2.87	(49.13)	144
	$^{1}H^{33}S$	^{33}S	C_{cc}	25.66	24.43	24.21	24.30	(22.2)	−0.07	(22.27)	144
HCP	$^{1}H^{12}C^{31}P$	^{31}P	$C_{aa}=C_{bb}, C_{cc}=0$	45.63	42.70	41.91	42.12	43.64			145
	$^{1}H^{13}C^{31}P$	^{13}C	$C_{aa}=C_{bb}, C_{cc}=0$	10.80	9.91	9.73	9.79				
	$^{1}H^{12}C^{31}P$	^{1}H	$C_{aa}=C_{bb}, C_{cc}=0$	−2.14	−2.05	−2.02	−2.02				
HFCO	$^{1}H^{19}F^{12}C^{16}O$	^{1}H	C_{aa}	−9.86	−9.29	−9.17	−9.15		0.18		
	$^{1}H^{19}F^{12}C^{16}O$	^{1}H	C_{bb}	0.96	0.95	0.95	0.95				
	$^{1}H^{19}F^{12}C^{16}O$	^{1}H	C_{cc}	−0.94	−0.89	−0.88	−0.88				
	$^{1}H^{19}F^{12}C^{16}O$	^{19}F	C_{aa}	148.10	152.70	159.12	159.50		0.89		
	$^{1}H^{19}F^{12}C^{16}O$	^{19}F	C_{bb}	24.33	25.00	25.65	25.73				
	$^{1}H^{19}F^{12}C^{16}O$	^{19}F	C_{cc}	12.56	13.65	14.11	14.11				
	$^{1}H^{19}F^{13}C^{16}O$	^{13}C	C_{aa}	32.17	31.09	30.64	30.87		0.00		
	$^{1}H^{19}F^{13}C^{16}O$	^{13}C	C_{bb}	4.82	4.59	4.56	4.58				
	$^{1}H^{19}F^{13}C^{16}O$	^{13}C	C_{cc}	2.74	2.81	2.83	2.85				
	$^{1}H^{19}F^{12}C^{17}O$	^{17}O	C_{aa}	−64.74	−59.72	−58.42	−58.64		−0.17		
	$^{1}H^{19}F^{12}C^{17}O$	^{17}O	C_{bb}	−5.85	−5.51	−5.42	−5.44				
	$^{1}H^{19}F^{12}C^{17}O$	^{17}O	C_{cc}	−0.85	−0.96	−1.01	−1.01				
H_2C_2O	$^{1}H^{12}C^{16}O$	^{1}H	C_{aa}	−18.38	−19.69	−19.76	−19.60	−18.296	1.22	−19.52	139
	$^{1}H^{12}C^{16}O$	^{1}H	C_{bb}	−0.06	−0.05	−0.05	−0.05	−0.087	−0.02	−0.07	139
	$^{1}H^{12}C^{16}O$	^{1}H	C_{cc}	−1.22	−1.13	−1.13	−1.12	−1.156	0.05	−1.21	139
	$^{1}H^{12}C^{17}O$	^{17}O	C_{aa}	−105.82	−104.78	−101.93	−102.27		5.48		
	$^{1}H^{12}C^{17}O$	^{17}O	C_{bb}	−1.78	−1.75	−1.79	−1.79		−0.11		
	$^{1}H^{12}C^{17}O$	^{17}O	C_{cc}	−4.81	−4.42	−4.37	−4.38		−0.01		
	$^{1}H^{12}C^{13}C^{16}O$	$^{13}C_o$	C_{aa}	22.91	21.95	21.27	21.42		−3.45		
	$^{1}H^{12}C^{13}C^{16}O$	$^{13}C_o$	C_{bb}	1.60	1.51	1.48	1.50		0.05		
	$^{1}H^{12}C^{13}C^{16}O$	$^{13}C_o$	C_{cc}	0.86	0.85	0.85	0.86		0.02		
	$^{1}H^{13}C^{12}C^{16}O$	$^{13}C_h$	C_{aa}	63.24	71.90	73.73	74.47	(71)	0.03	(70.97)	146
	$^{1}H^{13}C^{12}C^{16}O$	$^{13}C_h$	C_{bb}	5.13	4.89	4.83	4.85	(4.1)	0.02	(4.08)	146
	$^{1}H^{13}C^{12}C^{16}O$	$^{13}C_h$	C_{cc}	5.34	4.76	4.71	4.73	(4.4)	−0.30	(4.7)	146

TABLE III. (*Continued.*)

Molecule	Isotopologue	Nucleus	Tensor element	RHF	CCSD	CCSD(T)	Extrap.	Exp.	Vib.	Emp. Eq.	Exp. Ref.
LiF	$^{7}Li^{19}F$	^{7}Li	$C_{aa} = C_{bb}, C_{cc} = 0$	1.63	1.76	1.79	1.80	2.2	− 0.02	2.51	121
	$^{7}Li^{19}F$	^{19}F	$C_{aa} = C_{bb}, C_{cc} = 0$	28.81	30.45	31.46	31.60	32.9	− 0.31	32.92	121
LiH	$^{7}Li^{1}H$	^{7}Li	$C_{aa} = C_{bb}, C_{cc} = 0$	9.94	9.99	10.00	10.15	10.025	− 0.11	10.13	147
	$^{7}Li^{1}H$	^{1}H	$C_{aa} = C_{bb}, C_{cc} = 0$	− 9.69	− 9.51	− 9.51	− 9.49	− 9.05	0.17	−9.22	147
N_2O	$^{14}N^{14}N^{16}O$	$^{14}N_{out}$	$C_{aa} = C_{bb}, C_{cc} = 0$	2.17	1.87	1.81	1.82	1.82			148
	$^{14}N^{14}N^{16}O$	$^{14}N_{in}$	$C_{aa} = C_{bb}, C_{cc} = 0$	2.95	2.64	2.57	2.58	3.06			148
	$^{14}N^{14}N^{17}O$	^{17}O	$C_{aa} = C_{bb}, C_{cc} = 0$	− 3.34	− 2.97	− 2.96	− 2.97				
OCS	$^{16}O^{32}S^{13}C$	^{13}C	$C_{aa} = C_{bb}, C_{cc} = 0$	3.47	3.24	3.16	3.17	3.1			149
	$^{16}O^{33}S^{12}C$	^{33}S	$C_{aa} = C_{bb}, C_{cc} = 0$	1.10	1.06	1.06	1.07	0.87			132
	$^{17}O^{32}S^{12}C$	^{17}O	$C_{aa} = C_{bb}, C_{cc} = 0$	− 2.31	− 2.18	− 2.16	− 2.16				
OF_2	$^{19}F^{16}O^{19}F$	^{19}F	C_{aa}	38.27	49.97	52.81	52.99	(42)	1.48	(40.52)	150
	$^{19}F^{16}O^{19}F$	^{19}F	C_{bb}	19.19	23.01	24.07	24.17	(22)	0.54	(21.46)	150
	$^{19}F^{16}O^{19}F$	^{19}F	C_{cc}	48.87	50.12	51.09	51.32	(49)	1.41	(47.59)	150
	$^{19}F^{17}O^{19}F$	^{17}O	C_{aa}	− 37.11	− 35.58	− 40.19	− 40.45		− 2.66		
	$^{19}F^{17}O^{19}F$	^{17}O	C_{bb}	− 9.27	− 8.36	− 8.49	− 8.54		− 0.21		
	$^{19}F^{17}O^{19}F$	^{17}O	C_{cc}	− 5.18	− 5.06	− 5.31	− 5.34		− 0.04		
H_4C_2O	$^{1}H^{12}C^{12}C^{16}O$	^{1}H	C_{aa}	− 1.49	− 1.40	− 1.38	− 1.37		0.09		
	$^{1}H^{12}C^{12}C^{16}O$	^{1}H	C_{bb}	− 2.38	− 2.34	− 2.33	− 2.32				
	$^{1}H^{12}C^{12}C^{16}O$	^{1}H	C_{cc}	− 0.29	− 0.28	− 0.28	− 0.27				
	$^{1}H^{13}C^{12}C^{16}O$	^{13}C	C_{aa}	6.26	6.20	6.23	6.27		0.11		
	$^{1}H^{13}C^{12}C^{16}O$	^{13}C	C_{bb}	2.91	2.96	2.97	2.99				
	$^{1}H^{13}C^{12}C^{16}O$	^{13}C	C_{cc}	1.45	1.54	1.55	1.57				
	$^{1}H^{12}C^{12}C^{17}O$	^{17}O	C_{aa}	0.76	0.82	0.81	0.80		− 0.27		
	$^{1}H^{12}C^{12}C^{17}O$	^{17}O	C_{bb}	− 3.57	− 3.67	− 3.72	− 3.74				
	$^{1}H^{12}C^{12}C^{17}O$	^{17}O	C_{cc}	1.20	0.80	0.75	0.74				
PN	$^{31}P^{14}N$	^{31}P	$C_{aa} = C_{bb}, C_{cc} = 0$	91.67	79.86	77.65	78.09	78.2	0.14	78.06	129
	$^{31}P^{14}N$	^{14}N	$C_{aa} = C_{bb}, C_{cc} = 0$	12.73	10.53	10.21	10.25	10.4	0.02	10.38	129
SO_2	$^{33}S^{16}O^{16}O$	^{33}S	C_{aa}	50.41	41.99	39.78	40.07	39.56	0.47	39.09	151
	$^{33}S^{16}O^{16}O$	^{33}S	C_{bb}	6.61	5.92	5.76	5.79	5.60	0.02	5.58	151
	$^{33}S^{16}O^{16}O$	^{33}S	C_{cc}	4.23	4.18	4.19	4.22	4.63	0.00	4.63	151
	$^{32}S^{17}O^{16}O$	^{17}O	C_{aa}	− 54.86	− 45.72	− 44.51	− 44.63	− 45.06	− 1.08	−43.98	151
	$^{32}S^{17}O^{16}O$	^{17}O	C_{bb}	− 6.09	− 5.35	− 5.32	− 5.33	− 5.57	0.10	−5.67	151
	$^{32}S^{17}O^{16}O$	^{17}O	C_{cc}	− 1.95	− 2.12	− 2.18	− 2.20	− 1.80	− 0.03	−1.77	151

[a]Average of values for two different rotational transitions.

are found in the supplementary material[23]); also excluded are those molecules for which the experimental values appear questionable—that is, those values that are given in parentheses in Table II. All errors are for the isotropic shielding constants $\sigma_{iso} = \frac{1}{3}\mathrm{Tr}\boldsymbol{\sigma}$ in ppm.

Given that the shielding scales vary widely from nucleus to nucleus and given that different types of nuclei pose different challenges to quantum chemistry, it would perhaps be advantageous to study each type of nucleus separately. However, the essential trends in the accuracy of the methodologies considered are captured by the errors taken over all nuclei simultaneously. For brevity, we therefore focus here on errors averaged over all nuclei in our benchmark set of 28 molecules, as given in Table IV. In the supplementary material,[23] errors are presented separately for the subsets consisting of nuclear shieldings for the 18 hydrogen nuclei, 17 carbon nuclei, 7 nitrogen nuclei, 14 oxygen nuclei, and 9 fluorine nuclei in the benchmark set.

In this study, four families of basis sets are considered: the basic cc-pVXZ basis sets, the aug-cc-pVXZ basis sets with additional diffuse functions, the cc-pCVXZ with additional compact core functions (for core correlation), and the aug-cc-pCVXZ with additional diffuse and compact functions. In the following, we first examine the importance of these additions to the cc-pVXZ basis sets for the accurate calculation of shielding constants.

From Table IV, we see that the addition of diffuse augmenting functions leads to only modest changes in the error measures for isotropic NMR shielding constants. The mean absolute errors, for example, are changed by less than 1 ppm on addition of diffuse functions to the triple- and quadruple-zeta basis sets. At the double-zeta level, larger changes occur, indicating a degree of compensation for basis-set incompleteness on the addition of diffuse functions. The relative unimportance of diffuse functions is expected since NMR shielding constants are known to be more sensitive to the core–valence than to the outer-valence description. From the mean errors in Table IV, we note that the addition of diffuse functions increases the values of the shielding constants.

As seen from Table IV, the inclusion of core functions has a larger effect on the shielding constants than the inclusion of diffuse functions—in particular, in the coupled-cluster

TABLE IV. Isotropic absolute NMR shielding constants: Statistical errors for the molecules in Table II (excluding molecules with empirical equilibrium values in parentheses, see text) relative to the empirical equilibrium results. Presented are MEs, MAEs, MxAEs, MREs (%), MAREs (%), and SDs.

Method	Basis	X	ME	MAE	MxAE	MRE	MARE	SD
RHF	cc-pVXZ	2	2.5	17.3	143.7	− 8.0	37.5	28.3
		3	− 7.9	19.3	165.6	− 21.8	51.9	34.6
		4	− 8.0	18.6	167.2	− 22.9	57.9	31.4
	cc-pCVXZ	2	− 2.6	19.2	174.9	− 14.4	41.8	35.4
		3	− 9.1	20.3	175.6	− 24.1	56.5	36.4
		4	− 10.5	20.7	169.9	− 25.9	62.5	35.9
	aug-cc-pVXZ	2	3.1	15.5	117.8	− 10.0	32.8	26.0
		3	− 7.3	18.9	155.7	− 20.8	50.0	32.8
		4	− 8.1	18.5	165.0	− 22.6	57.8	31.0
	aug-cc-pCVXZ	2	− 1.6	17.3	161.3	− 15.7	36.2	32.5
		3	− 8.8	20.0	170.8	− 23.8	55.6	35.0
		4	− 10.5	20.6	168.4	− 25.7	62.2	35.4
CCSD	cc-pVXZ	2	20.0	21.0	134.1	23.5	73.1	26.7
		3	4.9	6.3	72.4	2.5	15.3	12.2
		4	3.8	6.4	47.0	− 1.0	10.9	10.7
	cc-pCVXZ	2	14.6	15.7	124.5	17.2	57.9	19.8
		3	2.5	5.9	63.0	− 0.8	12.0	11.0
		4	0.7	5.5	42.3	− 4.7	12.3	8.1
	aug-cc-pVXZ	2	20.4	20.6	106.0	18.3	64.9	24.5
		3	5.8	6.5	57.3	2.7	15.5	10.5
		4	3.8	6.2	41.5	− 1.0	9.7	10.0
	aug-cc-pCVXZ	2	15.4	15.6	84.5	12.7	51.2	17.1
		3	3.0	5.7	48.3	− 1.4	9.8	9.1
		4	0.8	5.5	36.4	− 4.8	12.3	8.1
CCSD(T)	cc-pVXZ	2	20.3	21.7	129.1	28.0	78.4	27.0
		3	5.9	6.7	48.2	7.7	21.4	9.7
		4	4.6	5.3	58.2	4.1	10.2	10.9
	cc-pCVXZ	2	15.0	16.6	101.9	21.9	63.8	18.3
		3	3.5	4.4	38.6	4.6	13.5	6.8
		4	1.6	2.8	19.6	0.5	4.9	4.0
	aug-cc-pVXZ	2	20.9	21.0	125.6	22.5	70.2	25.5
		3	6.7	7.1	36.9	7.7	21.5	8.6
		4	4.6	5.2	56.4	4.0	9.1	10.5
	aug-cc-pCVXZ	2	16.0	16.2	71.0	17.0	56.9	16.8
		3	4.0	4.5	21.4	3.8	12.3	5.1
		4	1.7	2.9	14.8	0.4	4.4	3.5

calculations, for which core–valence basis sets are needed for a proper description of electron correlation. Again, the largest changes occur for double-zeta basis sets: on the order of 2 ppm for Hartree–Fock theory and 5 ppm for coupled-cluster theory. In the larger triple and quadruple-zeta basis sets, the addition of core-correlating functions still leads to significant changes in the mean errors. For the quadruple-zeta sets, these changes are about 2.5 ppm for RHF theory, 3.1 ppm for CCSD theory and 3.0 ppm for CCSD(T) theory. A closer inspection of the mean errors in Table IV also reveals that core functions have the opposite effect to diffuse functions, decreasing rather than increasing the shielding constants.

In short, we conclude that core functions are important for shielding calculations, which should be calculated using the cc-pCVXZ basis sets rather than the cc-pVXZ basis sets. Diffuse functions have the opposite effect to core functions and may be included with core functions (in the aug-cc-pCVXZ basis sets) but never without core functions (in the aug-cc-pVXZ basis sets). In a previous study of magnetizabilities and rotational g tensors[14] for the same set of molecules, diffuse functions were found to be important and core-correlating functions less important. In general, therefore, the aug-cc-pCVXZ basis sets are recommended for studies of magnetic properties.

Regarding the dependence of the calculated shielding constants on the cardinal number X, we first note that shieldings consistently decrease with increasing X, at all levels of theory. The decrease is large from the double- to triple-zeta level of theory and smaller as we go to the quadruple-zeta level of theory. The double-zeta basis sets give unacceptably large errors for coupled-cluster theory, for which the use of double-zeta basis sets (with mean absolute relative errors exceeding 70%) should be strongly discouraged except as part of a convergence study. Indeed, in the cc-pVDZ basis, the coupled-cluster results are no better than the Hartree–Fock results. It is remarkable that, by error cancellation, Hartree–Fock theory performs as well with the cc-pVDZ basis set as with the aug-cc-pCVQZ basis set.

Concerning the relative performance of the RHF, CCSD, and CCSD(T) models for shielding constants, we note from Table IV that the effect of electron correlation is to increase shieldings. The RHF model typically underestimates shieldings (especially for large basis sets), whereas the CCSD and CCSD(T) models overestimate the shieldings (especially for small basis sets). Comparing the electronic-structure models in the largest aug-cc-pCVQZ basis, we note that the CCSD model reduces the errors by a factor of four or more relative to the RHF model. At the CCSD(T) level of theory, the errors are further reduced by about a factor of two (except for the mean errors). However, a meaningful comparison between the CCSD and CCSD(T) results is difficult because of errors in the experimental values.

For the benchmarking of DFT shielding constants, we will use the all-electron CCSD(T)/aug-cc-pCV[TQ]Z level of theory, obtained by applying the extrapolation formulae of Eqs. (5) and (6) to the aug-cc-pCVTZ and aug-cc-pCVQZ results at the CCSD(T) level of theory.

In Table II, the RHF, CCSD, and CCSD(T) benchmark values are presented along with the available experimental data and empirical equilibrium results for the largest aug-cc-pCVQZ basis and the CCSD(T)/aug-cc-pCV[TQ]Z benchmark results. The errors calculated relative to the benchmark CCSD(T) data, the empirical equilibrium values and the experimental data are presented in Table V. The results follow the trends expected. The effect of adding vibrational corrections can be gauged by comparing the error measures calculated with experimental and empirical equilibrium values as reference. The result of their addition to the coupled-cluster values is a further striking reduction in the errors—for example, the mean absolute relative error of the benchmark set is reduced from 17.4% to 6.5%.

TABLE V. Statistical errors in calculated NMR shielding constants for the molecules in Table II relative to the CCSD(T) values (excluding O_3 and SO_2), the empirical equilibrium values and the experimental values (ppm). The empirical equilibrium and experimental reference data excludes those values in parentheses in Table II.

Ref.	Err.	RHF[a]	CCSD[b]	CCSD(T)[b]	CCSD(T)[c]
CCSD(T)	ME	− 12.0	0.1	0.9	0.0
	MAE	19.1	3.2	0.9	0.0
	MxAE	162.5	32.5	5.1	0.0
	MRE	− 28.1	− 2.9	2.6	0.0
	MARE	63.7	7.9	4.7	0.0
	SD	31.6	5.7	1.0	0.0
Emp. Eq.	ME	− 10.5	0.8	1.7	0.8
	MAE	20.6	5.5	2.9	2.7
	MxAE	168.4	36.4	14.8	12.1
	MRE	− 25.7	− 4.8	0.4	− 1.2
	MARE	62.2	12.3	4.4	6.5
	SD	35.4	8.1	3.5	3.2
Exp.	ME	− 4.3	7.0	7.8	7.0
	MAE	20.9	9.2	8.0	7.3
	MxAE	161.4	80.7	53.2	48.2
	MRE	− 39.1	− 14.8	− 6.9	− 3.7
	MARE	120.4	22.9	29.7	17.4
	SD	36.0	14.7	10.8	10.3

[a] aug-cc-pCVQZ values.
[b] All-electron aug-cc-pCVQZ values.
[c] All-electron aug-cc-pCV[TQ]Z values.

B. Spin–rotation constants

Table VI contains statistical errors for 37 spin–rotation tensor elements evaluated using the RHF, CCSD, and CCSD(T) models relative to the empirical equilibrium values. As for the shieldings, we present error measures taken over all types of nuclei; a breakdown of these errors into subsets over selected nuclear types may be found in the supplementary material.[23] Unfortunately, the errors in the experimental error bars for spin–rotation constants are often relatively large, making it impossible to benchmark properly the most accurate levels of theory considered in this study.

As for the NMR shielding constants, double-zeta basis sets are too small for the accurate calculation of spin–rotation constants, except at the uncorrelated Hartree–Fock level of theory, where no improvement (relative to experiment) is observed as we increase the cardinal number. At the coupled-cluster level of theory, all error measures are reduced by several factors as X increases from two to three. Some further improvement is also observed when X increases to four, but not consistently (probably because of remaining large uncertainties in the experimental values).

The addition of core-correlating functions is more important than the addition of diffuse functions, consistent with the observations for shielding constants. In the all-electron coupled-cluster calculations presented here, core–valence basis sets should anyway always be used, for a proper treatment of core correlation. Diffuse functions should only be added to basis sets with cardinal number greater than two, to ensure a flexible treatment of the outer-valence region.

Comparing the three computational models, we note that the error measures are reduced by several factors and, in some cases, by an order of magnitude as we go from the uncorrelated RHF level of theory to the correlated CCSD level of theory. However, we do not observe the usual reduction (by a few factors) in the errors as we include triple excitations in our description, at the CCSD(T) level of theory. In all probability, the small (but still significant) improvements observed are a reflection of the relatively large uncertainties in the experimental spin–rotation constants.

In Table III, benchmark all-electron CCSD(T)/aug-cc-pCV[TQ]Z values for the spin–rotation constants are presented along with experimental and empirical equilibrium values. Statistical error measures for the calculated spin–rotation constants with respect to these different sets of reference data are presented in Table VII. In all cases, the systematic reduction in errors from RHF to CCSD to CCSD(T) is obvious and the error measures for the extrapolated CCSD(T) results and those calculated in the largest basis set considered agree well. Comparison of the error measures relative to experimental and empirical equilibrium values shows the significance of vibrational corrections. For example, the maximum absolute error for CCSD(T)/aug-cc-pCV[TQ]Z is reduced from 27.8 to 4.8 kHz and the mean absolute relative error from 10.9% to 4.4% upon inclusion of these corrections.

TABLE VI. Spin–rotation constants: Statistical errors for the molecules in Table III (excluding molecules with empirical equilibrium values in parentheses, see text) relative to the empirical equilibrium results. Presented are MEs, MAEs, MxAEs, MREs (%), MAREs (%), and SDs.

Method	Basis	X	ME	MAE	MxAE	MRE	MARE	SD
RHF	cc-pVXZ	2	− 1.4	3.0	18.3	3.7	14.1	4.7
		3	1.0	2.7	25.8	5.3	10.9	5.3
		4	1.1	2.7	29.7	5.0	10.7	5.5
	cc-pCVXZ	2	− 0.8	3.1	17.3	5.7	14.1	4.8
		3	1.1	2.6	21.7	5.8	10.5	4.8
		4	1.4	2.8	30.2	5.7	10.9	5.9
	aug-cc-pVXZ	2	− 1.1	2.4	14.6	2.9	12.5	3.4
		3	1.0	2.9	31.2	5.0	11.3	6.0
		4	1.1	2.7	29.7	5.0	11.1	5.5
	aug-cc-pCVXZ	2	− 0.4	2.6	15.5	4.7	12.5	4.0
		3	1.2	2.8	27.8	5.6	11.0	5.6
		4	1.4	2.9	30.3	5.7	11.2	5.9
CCSD	cc-pVXZ	2	− 3.1	3.8	39.0	− 3.0	14.7	7.1
		3	− 0.4	1.0	3.9	− 0.5	6.7	1.1
		4	− 0.2	0.7	4.3	− 1.0	5.2	1.0
	cc-pCVXZ	2	− 2.5	3.3	32.9	− 0.9	13.3	6.0
		3	− 0.2	0.9	3.3	0.2	6.2	0.9
		4	0.2	0.8	6.3	− 0.1	5.1	1.2
	aug-cc-pVXZ	2	− 3.1	3.3	35.3	− 3.5	13.1	6.3
		3	− 0.6	0.9	3.5	− 1.1	6.2	0.9
		4	− 0.3	0.7	3.6	− 1.1	5.4	0.9
	aug-cc-pCVXZ	2	− 2.4	2.8	28.4	− 1.7	11.6	5.0
		3	− 0.3	0.8	3.2	− 0.1	5.7	0.8
		4	0.1	0.8	3.6	− 0.2	5.3	1.0
CCSD(T)	cc-pVXZ	2	− 3.1	3.9	36.9	− 3.6	15.0	6.8
		3	− 0.6	1.1	5.0	− 1.5	6.8	1.2
		4	− 0.4	0.7	5.8	− 1.9	5.2	1.0
	cc-pCVXZ	2	− 2.5	3.3	30.9	− 1.6	13.1	5.8
		3	− 0.4	0.8	4.6	− 0.8	5.9	0.9
		4	0.0	0.6	4.1	− 1.1	4.5	0.8
	aug-cc-pVXZ	2	− 3.2	3.4	36.2	− 4.2	13.2	6.4
		3	− 0.8	0.9	3.8	− 2.1	6.1	0.9
		4	− 0.5	0.7	5.7	− 2.1	5.1	1.0
	aug-cc-pCVXZ	2	− 2.6	2.8	29.3	− 2.5	11.3	5.2
		3	− 0.5	0.7	2.8	− 1.1	5.1	0.6
		4	− 0.1	0.5	3.5	− 1.2	4.5	0.7

VI. BENCHMARKING DFT FUNCTIONALS

Having established the accuracy of the all-electron CCSD(T)/aug-cc-CV[TQ]VZ benchmark set (denoted CCSD(T) benchmark set in the following) relative to experimental and empirical equilibrium values, we now demonstrate its utility for benchmarking other quantum-chemical methods. Density-functional theory, in particular, is reliant on the availability of accurate benchmark data to assess the reliability and accuracy of approximate exchange–correlation functionals. In the following, we benchmark a variety of functionals in the LDA, GGA, hybrid, and OEP hybrid categories.

For LDA, we take the usual combination of the Dirac exchange functional and the VWN5 correlation functional;[41,42] for GGA, we consider the widely used BLYP[43,44] and PBE[45] functionals and also the KT2[46] functional, designed specifically with NMR shielding constants in mind. For the hybrid-functional category, we consider the representative B3LYP,[47,48] PBE0,[51] and B97-3[50] functionals and the range-dependent exchange variant CAM-B3LYP functional.[52] For the hybrid functionals, we also consider the evaluation of the magnetic properties using the OEP method. The values obtained using these DFT functionals may be compared directly with the CCSD(T) benchmark set, without the need for vibrational corrections, or with empirical equilibrium or experimental data.

A. NMR shielding constants

We begin by considering the evaluation of isotropic NMR shielding constants using pure DFT; subsequently, we discuss hybrid DFT results, obtained with and without OEPs. Statistical error measures are presented in Table VIII relative to the CCSD(T) values (excluding O_3 and SO_2), the empirical

TABLE VII. Statistical errors in calculated spin–rotation constants for the molecules in Table III relative to the CCSD(T) values (excluding O_3), the empirical equilibrium values and the experimental values (kHz). The empirical equilibrium and experimental reference data exclude those values in parentheses in Table III.

Ref.	Err.	RHF[a]	CCSD[b]	CCSD(T)[b]	CCSD(T)[c]
CCSD(T)	ME	− 0.6	− 0.2	− 0.1	0.0
	MAE	2.0	0.4	0.1	0.0
	MxAE	29.8	6.8	1.3	0.0
	MRE	3.9	0.2	− 0.1	0.0
	MARE	9.8	2.0	0.7	0.0
	SD	4.4	0.9	0.2	0.0
Emp. Eq.	ME	1.4	0.1	− 0.1	0.0
	MAE	2.9	0.8	0.5	0.5
	MxAE	30.3	3.6	3.5	4.8
	MRE	5.7	− 0.2	− 1.2	− 1.3
	MARE	11.2	5.3	4.5	4.4
	SD	5.9	1.0	0.7	0.9
Exp.	ME	0.0	− 0.7	− 0.8	− 0.7
	MAE	1.8	1.4	1.4	1.4
	MxAE	13.5	24.7	27.6	27.8
	MRE	9.3	3.0	1.9	1.9
	MARE	15.7	11.6	11.1	10.9
	SD	2.8	3.5	3.9	4.0

[a]aug-cc-pCVQZ values.
[b]All-electron aug-cc-pCVQZ values.
[c]All-electron aug-cc-pCV[TQ]Z values.

equilibrium values and the experimental values (excluding values given in parentheses in Table II).

1. Pure DFT calculations

For the LDA functional, the error measures with respect to all reference data are large, as expected. For the widely used BLYP and PBE GGA functionals, the errors are only reduced by a small amount—for example, the mean absolute error relative to the CCSD(T) benchmark set for LDA is 28 ppm, which is only reduced to 26 and 23 ppm for the BLYP and PBE functionals, respectively.

The tendency of LDA and GGA functionals to underestimate shielding constants has been widely documented in the literature[9–13,46,56,58,59] and is reflected in the mean errors in Table VIII. The origin of this underestimation can be traced to a poor description of the paramagnetic contribution to the NMR shielding. This term has an inverse dependence on the occupied–virtual Kohn–Sham eigenvalue differences which, in comparison to those obtained from inversion methods using accurate electronic densities such as Zhao–Morrison–Parr, Wu–Yang, or Lieb maximization, tend to be too small. The paramagnetic contribution therefore becomes too negative and the overall shielding constant too low—see, for example, Ref. 58.

Motivated by the fact that LDA and GGA functionals underestimate the magnitude of intershell peak structures, Keal and Tozer[46,152] developed a series of functionals designed to correct the exchange–correlation potentials in this region with the aim of improving the calculation of NMR shielding constants. Indeed, the KT2 error measures reported in Table VIII show a substantial improvement over the other GGA functionals—in particular, the mean absolute error relative to the CCSD(T) values is reduced to 10 ppm, almost one third of the LDA value. Moreover, the KT2 functional has consistently the lowest error measures of all DFT exchange–correlation functionals in Table VIII. A comparison of the KT2 errors relative to the empirical equilibrium values with the corresponding coupled-cluster errors in Table V allows us to put this achievement in context. Whereas the KT2 functional systematically underestimates the shielding constants with mean and mean absolute errors of −8.0 and 9.4 ppm, respectively, coupled-cluster theory overestimates the shielding

TABLE VIII. Isotropic NMR shielding constants: Statistical errors for the DFT/aug-cc-pCVQZ results relative to the CCSD(T)/aug-cc-pCV[TQ]Z benchmark data set (excluding O_3 and SO_2), empirical equilibrium values and experimental values. The empirical equilibrium and experimental reference data exclude those values in parentheses in Table II.

Ref.	Err.	LDA	BLYP	PBE	KT2	B3LYP	B97-2	B97-3	PBE0	CAM
CCSD(T)	ME	− 28.3	− 25.7	− 23.1	− 9.6	− 23.4	− 17.7	− 20.5	− 20.1	− 22.1
	MAE	28.3	25.8	23.2	10.2	23.5	17.8	20.6	20.2	22.2
	MxAE	225.2	194.4	182.4	91.4	141.7	113.1	114.6	121.1	139.1
	MRE	− 50.7	− 34.3	− 33.6	− 5.8	− 34.8	− 27.1	− 32.1	− 33.1	− 37.9
	MARE	98.8	79.8	71.5	19.4	79.4	56.4	72.4	69.6	81.6
	SD	38.4	31.1	29.5	16.2	27.8	22.0	25.0	25.6	28.6
Emp. Eq.	ME	− 25.3	− 23.1	− 20.7	− 8.0	− 20.9	− 15.9	− 18.2	− 17.8	− 19.6
	MAE	25.4	23.4	20.9	9.4	21.1	16.2	18.5	18.0	20.1
	MxAE	221.3	190.5	178.5	87.4	137.8	111.1	123.9	130.4	148.4
	MRE	− 31.7	− 21.6	− 21.5	− 3.6	− 23.9	− 19.3	− 23.4	− 23.6	− 26.6
	MARE	80.3	67.2	59.7	16.7	67.6	49.4	61.7	59.3	69.3
	SD	39.6	32.5	30.7	14.7	29.1	23.6	26.5	27.0	29.9
Exp.	ME	− 19.1	− 16.9	− 14.5	− 1.8	− 14.7	− 9.7	− 12.0	− 11.6	− 13.4
	MAE	20.3	17.6	15.4	5.7	15.8	11.3	13.8	13.7	15.9
	MxAE	177.0	146.2	134.2	43.2	122.7	104.2	117.0	123.5	141.5
	MRE	105.8	69.7	68.4	30.7	48.4	31.7	35.2	40.0	48.8
	MARE	239.9	176.6	162.5	36.9	173.7	122.1	157.7	154.9	182.2
	SD	33.7	26.5	24.8	9.2	24.5	19.3	22.6	22.8	25.8

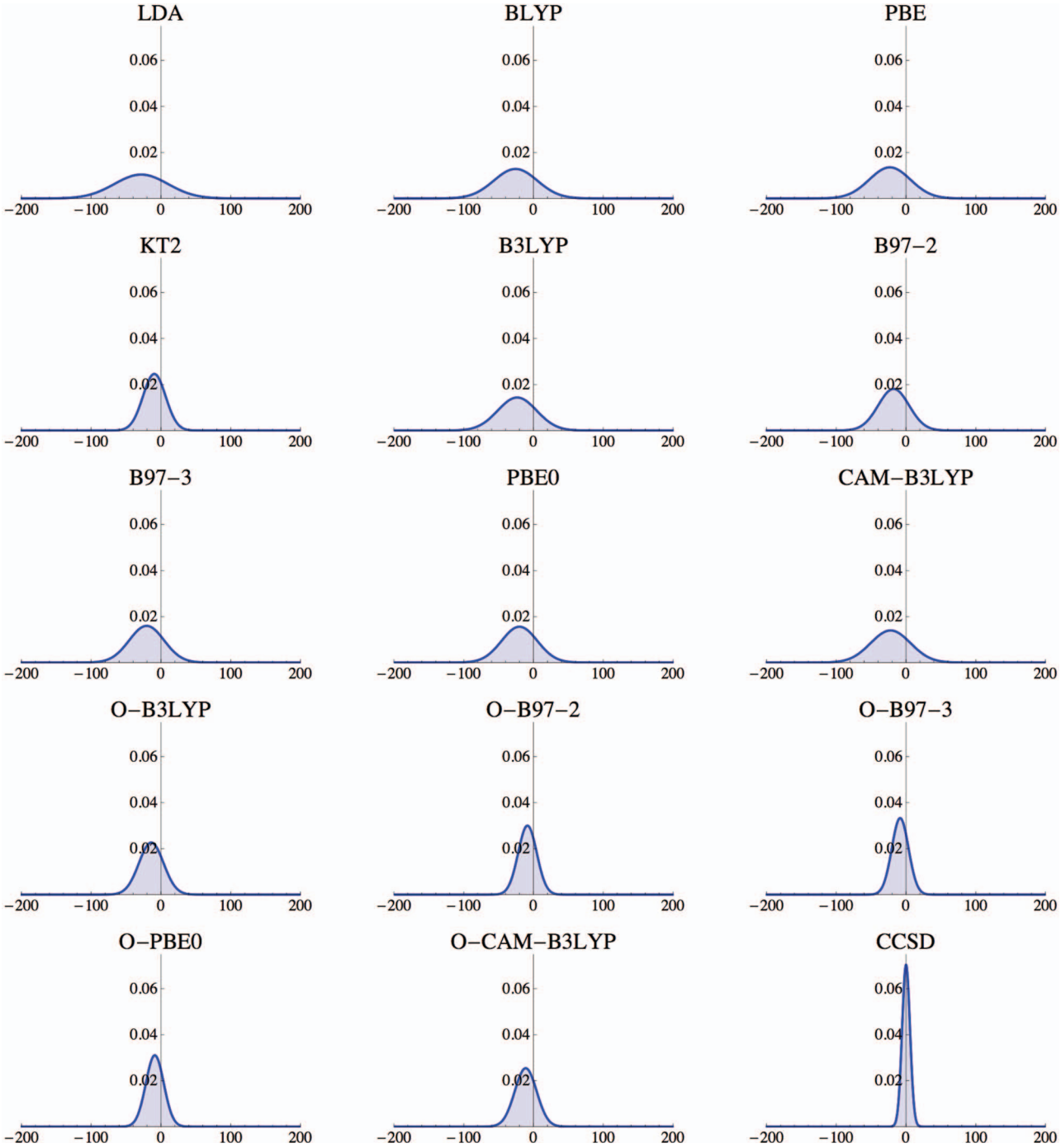

FIG. 1. Normal distributions of the errors in NMR shielding constants calculated in the aug-cc-pCVQZ basis relative to the CCSD(T)/aug-cc-pCV[TQ]Z benchmark data set for all molecules except O_3 and SO_2.

constants slightly, with mean and mean absolute errors of 1.7 and 2.9 ppm, respectively, for the CCSD(T) model and 0.8 and 5.5 ppm, respectively, for the CCSD model.

In Figure 1, we present the normal distributions of the errors in DFT shielding constants calculated in the aug-cc-pCVQZ basis set relative to the CCSD(T)/aug-cc-pCV[TQ]Z benchmark data set (excluding O_3 and SO_2), on a scale set to accommodate the more modest accuracy of the CCSD model. The main trends in the data are clearly reflected in these plots, the DFT methods systematically underestimating the shielding constants with relatively large standard deviations. The improvement of the KT2 functional over the other standard DFT functionals is clearly visible.

In Figure 2, the mean absolute errors of the shielding constants are represented graphically for the individual types of nuclei. Except for the nitrogen shieldings, the traditional LDA and GGA functionals perform considerably worse than the RHF model—in particular, for fluorine and oxygen. We also note that the KT2 functional consistently outperforms the other GGA functionals, for all nuclear types. Due to the differences in the shielding scales, it is difficult to discern the quality of the ^{1}H shielding constants from

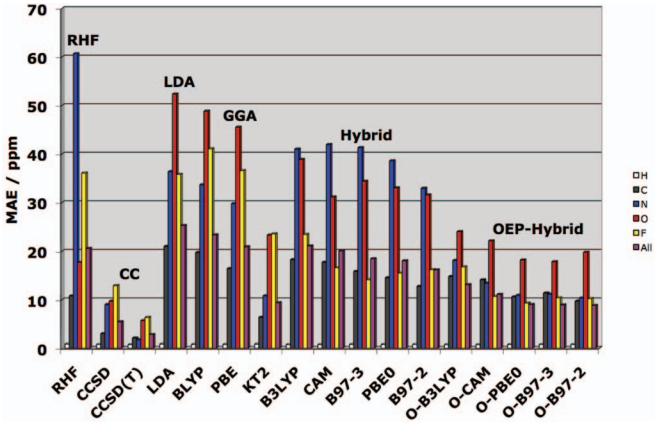

FIG. 2. Mean absolute errors (in ppm) for NMR shielding constants relative to empirical equilibrium values (excluding those in parenthesis in Table II) for H (white), C (grey), N (blue), O (red), and F (yellow). The total mean absolute errors over all nuclear types are shown by the purple bars. The DFT methodologies are arranged in the categories LDA, GGA, hybrid, and OEP-hybrid.

Figure 2. For ^{1}H shielding constants the mean absolute errors relative to empirical equilibrium values for RHF, CCSD, and CCSD(T) are 0.85, 0.78, and 0.75 ppm, respectively. While this follows the usual systematic trend it is noteworthy that the calculation of proton shielding constants is relatively unproblematic for all of the methods considered. For the density-functional approximations, LDA and KT2 give little improvement over RHF with mean absolute errors of 0.85 and 0.83 ppm relative to the empirical equilibrium values, respectively. All of the other methods give mean absolute errors in the range 0.74–0.78 ppm.

2. Hybrid DFT calculations

Here we consider standard global hybrid density functionals such as B3LYP,[47,48] B97-2,[49] B97-3,[50] and PBE0[51] and the ranged-separated hybrid CAM-B3LYP functional.[52] Errors for the B3LYP, B97-2, B97-3, PBE0, and CAM-B3LYP hybrid functionals considered in this study are presented in Table VIII. In contrast to the improvements typically observed for thermochemistry, it is clear that inclusion of Hartree–Fock exchange leads to only very modest improvements in the error measures. This behaviour is emphasized graphically in Figure 1, where the plots for hybrid functionals are remarkably similar to those for the pure functionals BLYP and PBE.

From Figure 2, we note that, with the inclusion of exact exchange, the hybrid functionals inherit the poor nitrogen performance of the RHF model. For the other atoms, however, the hybrid DFT approaches outperform the LDA and GGA functionals apart from the KT2 functional.

3. OEP functionals

As the use of the OEP procedure has attracted much attention in recent years, we have performed OEP calculations using the algorithm of Yang and Wu,[64] as described in Ref. 65. The aug-cc-pCVQZ basis has been used for the orbital and potential expansions, yielding smooth Kohn–Sham potentials and little sensitivity of the calculated NMR shielding constants to variations in the regularization parameter in the range 10^{-5}–10^{-8}. When the OEP method is applied to orbital-dependent hybrid functionals, the corresponding energy is minimized under the constraint that the exchange–correlation contribution to the Kohn–Sham matrix is a local multiplicative operator rather than a hybrid of local and nonlocal components. As a result, the magnetic Hessian becomes diagonal and the response equations become uncoupled, as in LDA and GGA theories. When the electronic energy and magnetic properties are evaluated in this manner, we prefix the parent functional with O to indicate an OEP evaluation.

Application of the OEP method leads to a consistent reduction in the error measures relative to the parent approximation, see Table IX. For example, the mean and mean absolute errors for B97-3 relative to the CCSD(T) benchmark set are reduced from −20.5 and 20.6 ppm, respectively, to −8.3 and 10.0 ppm. These values are comparable with those obtained for the KT2 functional, which was designed specifically with this property in mind. This improvement and its significance relative to the accuracy of the CCSD model is captured in the corresponding normal distributions presented in Figure 1. Finally, from Figure 2, we note that OEPs consistently improve upon all hybrid functionals—in particular, for the nitrogen shieldings.

4. Vibrational corrections

For all of the DFT results presented, a comparison of the error measures relative to the experimental and empirical equilibrium values reveals a striking trend: consideration of vibrational corrections worsen the quality of the DFT results. This trend is summarized in Figure 3 for the mean absolute

TABLE IX. Isotropic NMR shielding constants: Statistical errors for the DFT-OEP/aug-cc-pCVQZ results relative to the CCSD(T)/aug-cc-pCV[TQ]Z benchmark data set (excluding O_3 and SO_2), empirical equilibrium values and experimental values. The empirical equilibrium and experimental reference data exclude the values in parentheses in Table II.

Ref.	Err.	O-B3LYP	O-B97-2	O-B97-3	O-PBE0	O-CAM
CCSD(T)	ME	−13.9	−8.6	−8.3	−8.8	−11.1
	MAE	14.2	10.4	10.0	10.1	12.2
	MxAE	116.8	91.2	81.1	86.6	107.1
	MRE	−33.6	−26.8	−30.7	−31.7	−37.7
	MARE	50.3	34.7	38.7	39.7	51.1
	SD	17.6	13.3	12.0	12.9	15.7
Emp. Eq.	ME	−12.9	−8.2	−7.9	−8.3	−10.5
	MAE	13.1	8.9	9.0	9.0	11.1
	MxAE	112.9	87.3	77.2	82.6	103.2
	MRE	−18.9	−14.7	−16.7	−17.5	−20.1
	MARE	43.2	26.8	30.8	30.9	40.5
	SD	18.3	13.7	12.1	13.5	16.2
Exp.	ME	−6.7	−2.1	−1.7	−2.1	−4.3
	MAE	8.9	6.1	6.7	6.7	8.4
	MxAE	68.6	43.0	32.9	38.4	58.9
	MRE	55.2	39.5	46.3	48.9	64.7
	MARE	121.8	76.5	91.8	94.5	124.9
	SD	12.3	8.2	7.3	8.4	10.1

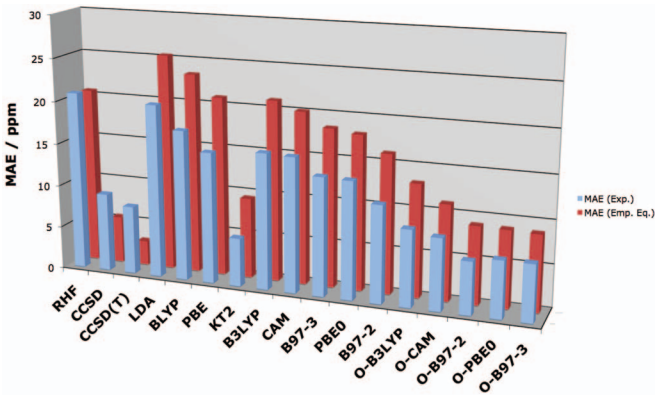

FIG. 3. Mean absolute errors (in ppm) for NMR shielding constants relative to experimental (blue) and empirical equilibrium values (red) over all nuclei (excluding those indicated by parentheses in Table II). The inclusion of vibrational corrections in the empirical equilibrium values leads to a degradation of the quality of the RHF and DFT results but to a notable improvement for the CCSD and CCSD(T) methods.

errors of all methods considered relative to empirical equilibrium and experimental values. The degradation of the DFT methods upon consideration of the vibrational corrections sharply contrasts the behaviour of the *ab initio* CCSD and CCSD(T) methods, for which inclusion of vibrational corrections further enhance the already high accuracy obtained.

B. Spin–rotation constants

In many respects, the performance of the density-functional approximations for spin–rotation constants resembles that for shielding constants. However, because of a delicate balance between the electronic and nuclear contributions to the spin–rotation constants in Eq. (4), high accuracy may be more difficult to achieve.

The error measures for standard density-functional approximations are presented in Table X. As expected, the LDA and GGA functionals offer relatively poor accuracy compared to either the CCSD(T) benchmark or empirical equilibrium results. Moreover, unlike for the shielding constants, the KT2 functional offers only a modest improvement over the other GGA functionals. For the hybrid approaches, a general but small improvement is observed, with the error measures showing consistent but minor improvements over the GGA functionals relative to all reference data.

The similarity in performance of the DFT methods for spin–rotation constants is placed in context in Figure 4, where the normal distributions for the various functionals are remarkably similar and show a tendency to overestimate the spin–rotation constants. Clearly, this property remains a challenge for DFT, and the accuracy achieved is modest when compared with the CCSD method.

In Table XI, the spin–rotation error measures for the application of the OEP method to the hybrid functionals are presented. A consistent improvement upon the parent functional is observed, in line with the observations for NMR shieldings. However, the improvements are modest, as illustrated in Figure 4. Furthermore, as for all DFT approaches, inclusion of vibrational corrections leads to larger error measures. This behaviour contrasts sharply with the situation for coupled-cluster theory, where vibrational corrections lead to consistent improvements and are essential for reliable comparisons with experimental data.

In Figure 5, mean absolute errors in the spin–rotation constants are represented graphically for individual nuclear types. The fluorine tensor elements are particularly problematic. The GGA and hybrid functionals, in particular, perform worse than RHF theory for fluorine; some improvement is observed with the OEP functionals. However, since relatively few fluorine data are included in our dataset, these large

TABLE X. Spin–rotation constants: Statistical errors for the DFT/aug-cc-pCVQZ results relative to the CCSD(T)/aug-cc-pCV[TQ]Z benchmark data set (excluding O_3), empirical equilibrium values and experimental values. The empirical equilibrium and experimental data exclude the values in parentheses in Table III.

Ref.	Err.	LDA	BLYP	PBE	KT2	B3LYP	B97-2	B97-3	PBE0	CAM
CCSD(T)	ME	1.1	1.5	1.3	1.2	0.9	0.8	0.7	0.7	0.6
	MAE	2.9	3.0	2.7	2.2	2.3	1.9	2.0	2.0	2.0
	MxAE	65.0	53.1	55.9	63.5	44.8	43.8	43.4	36.8	32.9
	MRE	6.4	6.2	5.2	2.3	5.7	3.7	4.6	4.6	5.6
	MARE	14.1	16.9	14.9	12.3	13.1	11.0	11.4	10.6	10.3
	SD	7.9	7.0	6.8	6.8	5.5	4.8	5.0	5.0	4.8
Emp. Eq.	ME	2.1	2.6	2.3	2.0	2.4	2.0	2.1	2.0	2.1
	MAE	3.2	3.9	3.5	3.0	3.5	2.9	3.1	3.0	3.0
	MxAE	34.5	53.5	44.3	64.0	45.3	44.2	43.9	37.3	29.8
	MRE	2.5	5.2	3.3	1.2	5.1	3.1	3.9	3.4	4.7
	MARE	11.3	11.4	10.9	7.7	10.2	8.9	9.6	9.4	9.0
	SD	6.6	9.7	8.3	10.9	8.2	7.8	7.9	7.0	6.2
Exp.	ME	1.2	1.4	1.2	0.8	1.1	0.8	0.8	0.8	0.9
	MAE	3.0	2.8	2.5	2.0	2.4	2.1	2.1	2.0	2.0
	MxAE	34.3	25.3	20.5	35.7	17.0	16.0	15.6	16.5	19.4
	MRE	6.9	8.1	6.6	4.4	8.3	6.5	7.3	7.1	8.1
	MARE	16.6	15.4	14.6	11.9	13.6	12.5	12.9	12.5	13.1
	SD	5.6	5.0	4.2	5.3	3.7	3.0	3.2	3.0	3.3

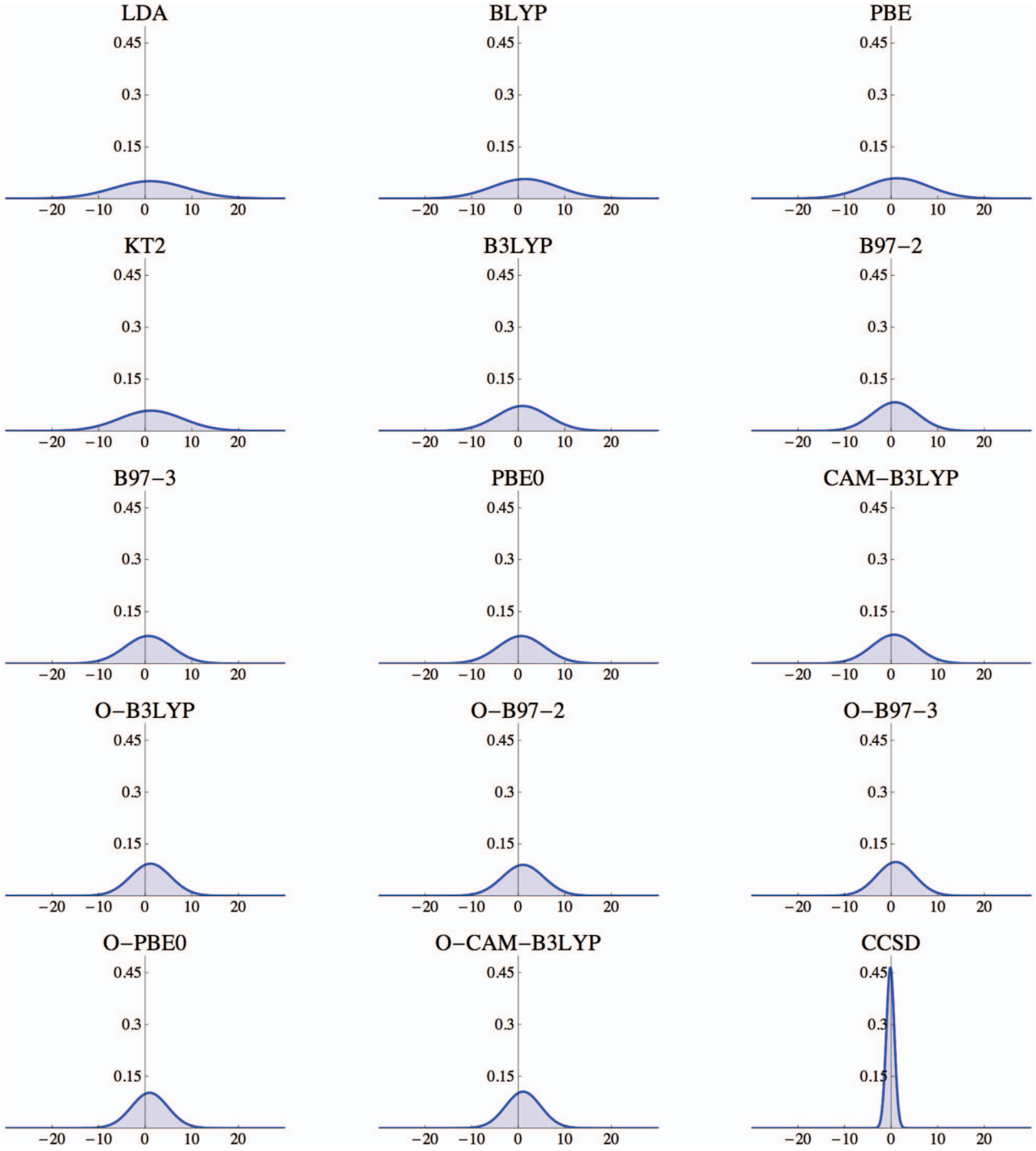

FIG. 4. Normal distributions of the errors in spin–rotation constants calculated in the aug-cc-pCVQZ basis relative to the CCSD(T)/aug-cc-pCV[TQ]Z benchmark data set for all molecules except O_3 SO_2.

errors do not dominate the statistics over all molecules. For the remaining nuclei, we note a fairly uniform performance of all DFT approaches for carbon and hydrogen; for nitrogen and oxygen, the KT2 and OEP functionals perform slightly better than other functionals.

VII. KS[CCSD] AND KS[CCSD(T)] CALCULATIONS

Throughout this paper, we have followed the common practice of evaluating the Kohn–Sham magnetic response properties with standard density-functional approximations, thereby neglecting the fact that, in the presence of a magnetic field, the exchange–correlation energy is a functional of not only the charge density ρ but also the paramagnetic current density $\mathbf{j}_p$.[153,154] Formally, this means that the evaluation of magnetic properties requires an implementation of current-density functional theory (CDFT). Unfortunately, relatively few CDFT functionals have been developed for practical use.[155–160] Many of these are specific parametrizations of the Vignale–Rasolt–Geldart (VRG) form.[155,156]

TABLE XI. Spin–rotation constants: Statistical errors for the DFT-OEP/aug-cc-pCVQZ results relative to the CCSD(T)/aug-cc-pCV[TQ]Z benchmark data set (excluding O_3), empirical equilibrium values and experimental values. The empirical equilibrium and experimental reference data exclude the values in parentheses in Table III.

Ref.	Err.	O-B3LYP	O-B97-2	O-B97-3	O-PBE0	O-CAM
CCSD(T)	ME	1.2	1.0	1.0	1.0	1.1
	MAE	1.9	1.7	1.6	1.6	1.7
	MxAE	32.4	29.5	26.3	29.6	28.4
	MRE	2.8	0.9	0.9	1.1	2.1
	MARE	12.2	10.5	10.5	9.8	10.7
	SD	4.3	4.4	4.1	3.9	3.8
Emp. Eq.	ME	1.7	1.4	1.3	1.3	1.4
	MAE	2.3	1.9	1.7	1.7	1.9
	MxAE	30.7	30.0	24.6	20.3	20.4
	MRE	2.6	0.8	0.8	0.5	1.8
	MARE	7.7	6.5	6.5	6.4	6.7
	SD	5.8	5.4	4.8	4.4	4.5
Exp.	ME	0.6	0.4	0.3	0.3	0.5
	MAE	1.5	1.2	1.3	1.4	1.7
	MxAE	16.6	12.7	15.0	16.5	20.1
	MRE	5.4	3.7	3.6	3.6	4.5
	MARE	11.5	10.6	10.7	10.2	11.0
	SD	2.6	2.0	2.3	2.6	3.2

Lee *et al.*[157] have presented an implementation of the VRG functional with an exponential parametrization in the context of response theory. However, the need for the VRG correction is difficult to gauge from their results, bearing in mind that the correction was applied to functionals, such as LDA and BLYP, which are already substantially in error for NMR shielding constants, see Table VIII. For the molecules studied by Lee *et al.*[157] (HF, CO, N_2, F_2, H_2O, and CH_4), the largest VRG corrections to the shieldings occur in molecules where a magnetic field perpendicular to the bond axis is expected to induce a strong paramagnetic current. In N_2 and CO, for example, the magnitude of the VRG corrections to the BLYP values are 6 ppm in N_2 and 5 and 7 ppm for C and O in CO, respectively. It should be noted, however, that these corrections move the already erroneous BLYP results further away from the experimental values. For molecules, such as HF and H_2O, the corresponding VRG corrections are much smaller: 0.03 and 1.1 ppm for H and F in HF, and 0.01 and 1.2 ppm for H and O in H_2O, respectively.[157] Clearly, open questions remain as to whether VRG corrections can be fruitful for more accurate density-functional approximations and also how accurate the VRG form is for describing this contribution.

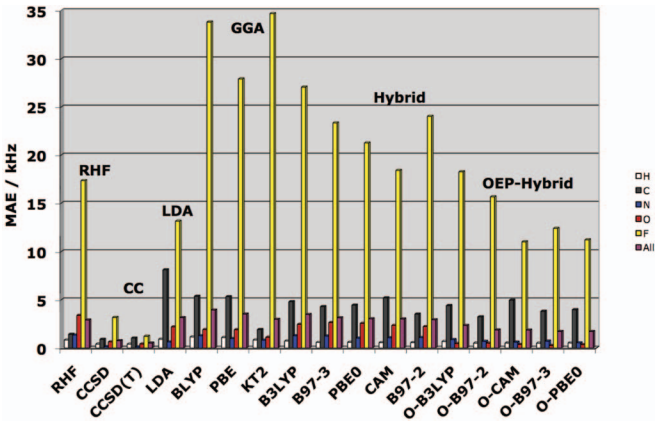

FIG. 5. Mean absolute errors (in Hz) for spin–rotation constants relative to empirical equilibrium values (excluding those values in parentheses in Table III), presented for H (white), C (grey), N (blue), O (red), and F (yellow). The total mean absolute errors over all nuclear types are shown by the purple bars. The DFT methodologies are arranged in the categories LDA, GGA, hybrid, and OEP-hybrid.

In this study, we consider instead how accurately NMR shielding constants and spin–rotation constants may be determined under the usual assumption that $E_{xc}[\rho, \mathbf{j}_p] \approx E_{xc}[\rho]$. Since we are able to calculate accurate charge densities from the CCSD and CCSD(T) models, it is interesting to consider the evaluation of these molecular properties from Kohn–Sham potentials, orbitals and eigenvalues constructed to yield these charge densities. For this purpose, we employ the procedure proposed by Wu and Yang[81] (which is equivalent to the Lieb maximization for non-interacting systems) with the same choices of potential-expansion basis, TSVD regularization and optimization algorithm as previously discussed for OEPs. Once these accurate Kohn–Sham quantities have been determined from the CCSD and CCSD(T) densities, we evaluate the response properties in the usual uncoupled DFT manner, denoting the results KS[CCSD] and KS[CCSD(T)], respectively. (Note that, in our previous work,[14] we used the alternative notation WY[CCSD] and WY[CCSD(T)].) By comparing the KS[CCSD] and KS[CCSD(T)] results with the corresponding coupled-cluster and DFT results, we can gauge the extent to which improving the quality of the approximate functionals and hence charge densities alone (without introducing currents) can lead to improvements in the Kohn–Sham magnetic response properties.

For the subset of molecules HF, CO, N2, H_2O, HCN, NH_3, CH_2O, CH_4, CH_3F, FCN, H_2S, HCP, N_2O, and PN, we present the KS[CCSD] and KS[CCSD(T)] errors relative to the corresponding coupled-cluster results in the aug-cc-pCVQZ basis set in Table XII. It is noteworthy that the KS[CC] error measures are close to those of the OEP-based methods over the same subset. For example, whereas the KS[CCSD] and KS[CCSD(T)] mean absolute errors relative to CCSD and CCSD(T) results for the subset of molecules are 6.1 and 10.9 ppm, respectively, the corresponding O-B97-2 errors are 7.4 and 9.7 ppm. This observation indicates that the errors in the OEP shieldings arise predominantly from the neglect of currents and their effective potentials in the DFT treatment rather from a poor description of densities and their effective potentials. Clearly, a re-examination of the impact of CDFT corrections on shieldings is worthwhile.

For the spin–rotation constants, the KS[CCSD] and KS[CCSD(T)] errors are likewise comparable with those of the OEP methods. For example, while the O-PBE0 functional gives mean absolute errors of 1.6 and 1.7 kHz, respectively, relative to the CCSD and CCSD(T) results for the subset of molecules, the corresponding KS[CCSD] and KS[CCSD(T)] errors are 1.6 and 1.5 kHz. Similar observations were made in our previous study[14] of magnetizabilities and rotational g tensors. The impact of CDFT corrections and assessment of their accuracy will form part of a future study.

TABLE XII. Absolute isotropic shielding constants (ppm) and spin–rotation constants (kHz): Statistical errors in KS[CC] values relative to the corresponding CC values (all-electron/aug-cc-pCVQZ values).

	NMR isotropic shieldings		Spin–rotation constants	
	KS[CCSD]	KS[CCSD(T)]	KS[CCSD]	KS[CCSD(T)]
ME	− 2.0	− 10.7	1.3	1.2
MAE	6.1	10.9	1.6	1.5
MxAE	41.7	53.6	48.6	25.2
MRE	− 5.0	− 29.0	1.1	2.6
MARE	41.3	39.4	6.3	7.4
SD	9.8	13.2	6.2	3.6

VIII. CONCLUSIONS

We have performed a benchmark study of NMR shielding constants and spin–rotation tensors, complementing our previous work on magnetizabilities and rotational *g* tensors. We have collected experimental shielding constants and spin–rotation tensors from the literature; all data have been carefully assessed for reliability and accuracy, to ensure suitability for benchmarking. Vibrational corrections have been calculated at the B3LYP level of theory to enable a rigorous comparison of empirical and calculated equilibrium values of the constants.

In preparation for the benchmark study of various density-functional approximations, we performed an analysis of the errors at the RHF, CCSD, and CCSD(T) levels of theory for the two properties of interest. At the extrapolated all-electron CCSD(T)/aug-cc-pCV[TQ]Z level of theory, the calculated constants are of a quality comparable to that of most measurements. This level of theory was therefore selected as reference for the subsequent benchmarking of the various DFT functionals.

For the NMR shielding constants and the spin–rotation tensors, the various DFT approximations improve slightly (but not uniformly) upon the Hartree–Fock theory, struggling to achieve an accuracy and reliability comparable with that of CCSD theory. The DFT approximations generally underestimate shielding constants; for the spin–rotation constants, the errors are less systematic. Moreover, the inclusion of vibrational corrections tends to worsen the agreement with experimental values.

Comparing the various DFT approximations, we observe a general improvement from LDA to GGA exchange–correlation functionals. Hybrid functionals further improve the results but not consistently. In particular, the difficulties that the RHF method has in describing nitrogen shieldings are inherited by the hybrid methods, which perform worse than the LDA and GGA functionals for nitrogen shieldings. As previously observed for magnetizabilities and rotational *g* values, the quality of the calculated constants is consistently improved by the use of OEPs.

To examine the importance of current-density contributions to magnetic properties in Kohn–Sham theory, we have carried out KS[CCSD] and KS[CCSD(T)] calculations for the shielding constants and spin–rotation tensors. These calculations, in which the Kohn–Sham potential exactly reproduces the coupled-cluster density, provide a quality broadly similar to that of the OEP calculations, indicating that the current-density contributions of CDFT are non-negligible and should be included in a consistent Kohn–Sham treatment of molecular magnetic properties.

ACKNOWLEDGMENTS

This work has been supported by the Norwegian research council through Grant Nos. 171185/V30 and 197446/V30 and the CeO Centre for Theoretical and Computational Chemistry through Grant No. 179568/V30. The research leading to these results has also received funding from the European Research Council under the European Union's Seventh Framework Programme (FP7/2007-2013)/ERC Grant agreement No. 267683. A.M.T. is also grateful for support from a Royal Society University Research Fellowship. The work in Mainz has been supported by the Deutsche Forschungsgemeinschaft and the Fonds der Chemischen Industrie. O.B.L. thanks Jonas Jusélius for assistance in the ACESII calculations. We thank Kenneth Ruud for clarifying discussions.

[1] R. G. Parr and W. Yang, *Density-Functional Theory of Atoms and Molecules* (Oxford University Press, 1989).
[2] W. Koch and M. C. Holthausen, *A Chemist's Guide to Density Functional Theory*, 2nd ed. (Wiley-VCH, 2001).
[3] G. D. Purvis and R. J. Bartlett, J. Chem. Phys. **76**, 1910 (1982).
[4] K. Raghavachari, G. W. Trucks, J. A. Pople, and M. Head-Gordon, Chem. Phys. Lett. **157**, 479 (1989).
[5] A. A. Auer, J. Gauss, and J. F. Stanton, J. Chem. Phys. **118**, 10407 (2003).
[6] M. E. Harding, M. Lenhart, A. A. Auer, and J. Gauss, J. Chem. Phys. **128**, 244111 (2008).
[7] A. A. Auer, J. Chem. Phys. **131**, 024116 (2009).
[8] E. Prochnow and A. A. Auer, J. Chem. Phys. **132**, 064109 (2010).
[9] G. Magyarfalvi and P. Pulay, J. Chem. Phys. **119**, 1350 (2003).
[10] T. W. Keal, D. J. Tozer, and T. Helgaker, Chem. Phys. Lett. **391**, 374 (2004).
[11] T. Kupka, Magn. Reson. Chem. **47**, 959 (2009).
[12] T. Kupka, M. Stachów, M. Nieradka, J. Kaminsky, and T. Pluta, J. Chem. Theory Comput. **6**, 1580 (2010).
[13] T. Kupka, M. Stachów, M. Nieradka, J. Kaminsky, T. Pluta, and S. P. A. Sauer, Magn. Reson. Chem. **49**, 231 (2011).
[14] O. B. Lutnæs, A. M. Teale, T. Helgaker, D. J. Tozer, K. Ruud, and J. Gauss, J. Chem. Phys. **131**, 144104 (2009).
[15] K. Ruud, T. Helgaker, K. L. Bak, P. Jørgensen, and H. J. A. Jensen, J. Chem. Phys. **99**, 3847 (1993).
[16] D. J. D. Wilson, C. E. Mohn, and T. Helgaker, J. Chem. Theory Comput. **1**, 877 (2005).
[17] J. Gauss, K. Ruud, and T. Helgaker, J. Chem. Phys. **105**, 2804 (1996).
[18] J. Gauss and J. F. Stanton, J. Chem. Phys. **103**, 3561 (1995).
[19] J. Gauss and J. F. Stanton, J. Chem. Phys. **104**, 2574 (1996).
[20] T. Helgaker, W. Klopper, H. Koch, and J. Noga, J. Chem. Phys. **106**, 9639 (1997).
[21] A. Halkier, T. Helgaker, P. Jørgensen, W. Klopper, H. Koch, J. Olsen, and A. K. Wilson, Chem. Phys. Lett. **286**, 243 (1998).
[22] A. Halkier, T. Helgaker, P. Jørgensen, W. Klopper, and J. Olsen, Chem. Phys. Lett. **302**, 437 (1999).
[23] See supplementary material at http://dx.doi.org/10.1063/1.4773016 for data and error analysis in other basis sets.
[24] R. T. Sharp and G. K. Horton, Phys. Rev. **90**, 317 (1953).
[25] J. D. Talman and W. F. Shadwick, Phys. Rev. **A 14**, 36 (1976).
[26] M. Levy, Proc. Natl. Acad. Sci. U.S.A. **76**, 6062 (1979).
[27] W. H. Flygare, Chem. Rev. **74**, 653 (1974).
[28] T. Helgaker, M. Jaszuński, and K. Ruud, Chem. Rev. **99**, 293 (1999).
[29] J. Gauss and J. F. Stanton, Adv. Chem. Phys. **123**, 355 (2002).
[30] W. H. Flygare and J. T. Lowe, J. Chem. Phys. **43**, 3645 (1965).
[31] F. London, J. Phys. Radium **8**, 397 (1937).

[32] DALTON, an *ab initio* electronic structure program, Release 2.0 2005, see http://www.kjemi.uio.no/software/dalton/dalton.html.
[33] ACESII, Mainz-Austin-Budapest-Version, 2007, see http://www.aces2.de.
[34] T. H. Dunning, J. Chem. Phys. **90**, 1007 (1989).
[35] R. A. Kendall, T. H. Dunning, and R. J. Harrison, J. Chem. Phys. **96**, 6796 (1992).
[36] D. E. Woon and T. H. Dunning, J. Chem. Phys. **100**, 2975 (1994).
[37] D. E. Woon and T. H. Dunning, J. Chem. Phys. **103**, 4572 (1995).
[38] A. Halkier, W. Klopper, T. Helgaker, and P. Jørgensen, J. Chem. Phys. **111**, 4424 (1999).
[39] F. Pawłowski, A. Halkier, P. Jørgensen, K. L. Bak, T. Helgaker, and W. Klopper, J. Chem. Phys. **118**, 2539 (2003).
[40] M. Heckert, M. Kállay, P. Tew, W. Klopper, and J. Gauss, J. Chem. Phys. **125**, 044108 (2006).
[41] P. Hohenberg and W. Kohn, Phys. Rev. **B136**, B864 (1964).
[42] S. H. Vosko, L. Wilk, and M. Nusair, Can. J. Phys. **58**, 1200 (1980).
[43] A. D. Becke, Phys. Rev. **A 38**, 3098 (1988).
[44] C. Lee, W. Yang, and R. G. Parr, Phys. Rev. **B 37**, 785 (1988).
[45] J. P. Perdew, K. Burke, and M. Ernzerhof, Phys. Rev. Lett. **77**, 3865 (1996).
[46] T. W. Keal and D. J. Tozer, J. Chem. Phys. **119**, 3015 (2003).
[47] P. J. Stephens, F. J. Devlin, C. F. Chabalowski, and M. J. Frisch, J. Phys. Chem. **98**, 11623 (1994).
[48] A. D. Becke, J. Chem. Phys. **98**, 5648 (1993).
[49] P. J. Wilson, T. J. Bradley, and D. J. Tozer, J. Chem. Phys. **115**, 9233 (2001).
[50] T. W. Keal and D. J. Tozer, J. Chem. Phys. **123**, 121103 (2005).
[51] C. Adamo and V. Barone, J. Chem. Phys. **110**, 6158 (1999).
[52] T. Yanai, D. P. Tew, and N. C. Handy, Chem. Phys. Lett. **393**, 51 (2004).
[53] P. J. Wilson and D. J. Tozer, Chem. Phys. Lett. **337**, 341 (2001).
[54] M. J. Allen, T. W. Keal, and D. J. Tozer, Chem. Phys. Lett. **380**, 70 (2003).
[55] P. J. Wilson and D. J. Tozer, J. Mol. Struct. **602**, 191 (2002).
[56] A. J. Cohen, Q. Wu, and W. Yang, Chem. Phys. Lett. **399**, 84 (2004).
[57] A. M. Teale, A. J. Cohen, and D. J. Tozer, J. Chem. Phys. **126**, 074101 (2007).
[58] A. M. Teale and D. J. Tozer, Chem. Phys. Lett. **383**, 109 (2004).
[59] W. Hieringer, F. Della Sala, and A. Görling, Chem. Phys. Lett. **383**, 115 (2004).
[60] A. V. Arbuznikov and M. Kaupp, Chem. Phys. Lett. **386**, 8 (2004).
[61] A. V. Arbuznikov and M. Kaupp, Chem. Phys. Lett. **391**, 16 (2004).
[62] A. V. Arbuznikov and M. Kaupp, Int. J. Quantum Chem. **104**, 261 (2005).
[63] O. B. Lutnæs, A. M. Teale, T. Helgaker, and D. J. Tozer, J. Chem. Theory Comput. **2**, 827 (2006).
[64] W. Yang and Q. Wu, Phys. Rev. Lett. **89**, 143002 (2002).
[65] Q. Wu and W. Yang, J. Theor. Comput. Chem. **2**, 627 (2003).
[66] S. Hirata, S. Ivanov, I. Grabowski, R. J. Bartlett, K. Burke, and J. D. Talman, J. Chem. Phys. **115**, 1635 (2001).
[67] R. J. Bartlett, I. Grabowski, S. Hirata, and S. Ivanov, J. Chem. Phys. **122**, 034104 (2005).
[68] V. N. Staroverov, G. E. Scuseria, and E. R. Davidson, J. Chem. Phys. **125**, 081104 (2006).
[69] V. N. Staroverov, G. E. Scuseria, and E. R. Davidson, J. Chem. Phys. **124**, 141103 (2006).
[70] D. Rohr, O. V. Gritsenko, and E. J. Baerends, J. Mol. Struct.:THEOCHEM **762**, 193 (2006).
[71] A. Heßelman, A. W. Götz, F. Della Sala, and A. Görling, J. Chem. Phys. **127**, 054102 (2007).
[72] C. Kollmar and M. Filatov, J. Chem. Phys. **127**, 114104 (2007).
[73] D. P. Joubert, J. Chem. Phys. **127**, 244104 (2007).
[74] C. Kollmar and M. Filatov, J. Chem. Phys. **128**, 064101 (2008).
[75] T. Heaton-Burgess, F. A. Bulat, and W. Yang, Phys. Rev. Lett. **98**, 256401 (2007).
[76] T. Heaton-Burgess and W. Yang, J. Chem. Phys. **129**, 194102 (2008).
[77] M. J. G. Peach, J. A. Kattirtzi, A. M. Teale, and D. J. Tozer, J. Phys. Chem. **A 114**, 7179 (2010).
[78] T. Helgaker and P. Jørgensen, Theor. Chim. Acta **75**, 111 (1989).
[79] P. Jørgensen and T. Helgaker, J. Chem. Phys. **89**, 1560 (1988).
[80] H. Koch, H. J. A. Jensen, P. Jørgensen, T. Helgaker, G. E. Scuseria, and H. F. Schaefer III, J. Chem. Phys. **92**, 4924 (1990).
[81] Q. Wu and W. Yang, J. Chem. Phys. **118**, 2498 (2003).
[82] K. Ruud, P.-O. Åstrand, and P. R. Taylor, J. Chem. Phys. **112**, 2668 (2000).
[83] C. J. Jameson, A. K. Jameson, D. Oppusunggu, S. Wille, P. M. Burell, and J. Mason, J. Chem. Phys. **74**, 81 (1981).
[84] S. G. Kukolich, J. Am. Chem. Soc. **97**, 5704 (1975).
[85] W. T. Raynes, Nucl. Magn. Reson. **7**, 1 (1978).
[86] D. Sundholm, J. Gauss, and A. Schäfer, J. Chem. Phys. **105**, 11051 (1996).
[87] C. Puzzarini, G. Cazzoli, M. E. Harding, J. Vázquez, and J. Gauss, J. Chem. Phys. **131**, 234304 (2009).
[88] R. E. Wasylishen, C. Connor, and J. O. Friedrich, Can. J. Chem. **62**, 981 (1984).
[89] K. Jackowski, W. Makulski, and W. Kominski, Magn. Reson. Chem. **40**, 563 (2002).
[90] C. J. Jameson, A. D. Dios, and A. K. Jameson, J. Chem. Phys. **95**, 9042 (1991).
[91] K. Jackowski, M. Wilczek, M. Pecul, and J. Sadlej, J. Phys. Chem. **A 104**, 5955 (2000).
[92] A. K. Jameson and C. J. Jameson, Chem. Phys. Lett. **134**, 461 (1987).
[93] D. K. Hindermann and C. D. Cornwell, J. Chem. Phys. **48**, 4148 (1968).
[94] R. E. Wasylishen and D. L. Bryce, J. Chem. Phys. **117**, 10061 (2002).
[95] R. E. Wasylishen, S. Mooibroek, and J. B. Macdonald, J. Chem. Phys. **81**, 1057 (1984).
[96] S. M. Bass, R. L. DeLeon, and J. S. Muenter, J. Chem. Phys. **86**, 4305 (1987).
[97] G. Cazzoli, L. Dore, C. Puzzarini, and S. Beninati, Phys. Chem. Chem. Phys. **4**, 3575 (2002).
[98] W. L. Meerts, F. H. De Leeuw, and A. Dymanus, Chem. Phys. **22**, 319 (1977).
[99] W. G. Schneider, H. J. Bernstein, and J. A. Pople, J. Chem. Phys. **28**, 601 (1958).
[100] J. C. Hindman, A. Svirmickas, and E. H. Appelman, J. Chem. Phys. **57**, 4542 (1972).
[101] I. J. Solomon, J. N. Keith, J. Kacmarek, and J. K. Raney, J. Am. Chem. Soc. **90**, 5408 (1968).
[102] C. J. Jameson, Nucl. Magn. Reson. **18**, 1 (1989).
[103] R. Cornet, B. M. Landsberg, and G. Winnewisser, J. Mol. Spectrosc. **82**, 253 (1980).
[104] K. D. Tucker, G. R. Tomasevich, and P. Thaddeus, Astrophys. J. **174**, 463 (1972).
[105] J. C. Hindman, J. Chem. Phys. **44**, 4582 (1966).
[106] C. J. Jameson, A. K. Jameson, and P. M. Burrell, J. Chem. Phys. **73**, 6013 (1980).
[107] H. Spiesecke and W. G. Schneider, J. Chem. Phys. **35**, 722 (1961).
[108] H. O. Kalinowski, S. Berger, and S. Braun, *^{13}C-NMR-Spektroskopie* (Thieme, Stuttgart, 1984).
[109] W. Kutzelnigg, U. Fleischer, and M. Schindler, *NMR Basic Principles and Progress* (Springer-Verlag, 1991), Vol. 23, p. 165.
[110] H. Günther, *NMR-Spektroskopie* (Thieme, Stuttgart, 1983).
[111] W. J. Middleton and W. H. Sharkey, J. Am. Chem. Soc. **81**, 803 (1959).
[112] G. Filipovich and G. V. D. Tiers, J. Phys. Chem. **63**, 761 (1959).
[113] B. R. Appleman and B. P. Dailey, Adv. Magn. Reson. **7**, 231 (1974).
[114] R. Ditchfield and P. D. Ellis, Chem. Phys. Lett. **17**, 342 (1972).
[115] F. S. Fawcett and R. D. Lipscomb, J. Am. Chem. Soc. **82**, 1509 (1960).
[116] S. P. Anderson, H. Goldwhite, D. Ko, and A. Letsou, J. Chem. Soc., Chem. Commun. **18**, 744 (1975).
[117] N. Muller and D. T. Carr, J. Phys. Chem. **A 67**, 112 (1963).
[118] E. L. Allred, D. M. Grant, and W. Goodlett, J. Am. Chem. Soc. **87**, 673 (1963).
[119] J. Firl and W. Runge, Angew. Chem. **85**, 671 (1973).
[120] H. J. Kolker and M. Karplus, J. Chem. Phys. **41**, 1259 (1964).
[121] R. Braunstein and J. W. Trischka, Phys. Rev. **98**, 1092 (1955).
[122] L. Wharton, L. P. Gold, and W. Klemperer, J. Chem. Phys. **37**, 2149 (1962).
[123] W. Makulski and K. Jackowski, J. Mol. Struct. **651–653**, 265 (2003).
[124] K. Jackowski, M. Jaszuński, W. Makulski, and J. Vaara, J. Magn. Reson. **135**, 444 (1998).
[125] J. W. Nebgen, F. I. Metz, and W. B. Rose, J. Am. Chem. Soc. **89**, 3118 (1967).
[126] T. Sugawara, Y. Kawada, M. Katoh, and H. Iwamura, Bull. Chem. Soc. Jpn. **52**, 3391 (1979).
[127] G. E. Maciel and G. B. Savitsky, J. Phys. Chem. **69**, 3925 (1965).
[128] E. Lippert and H. Prigge, Ber. Bunsenges. **67**, 415 (1963).
[129] J. Raymonda and W. Klemperer, J. Chem. Phys. **55**, 232 (1971).
[130] W. Makulski and K. Jackowski, J. Mol. Struct. **704**, 219 (2004).
[131] W. D. Phillips, W. E. Cooke, and D. Kleppner, Phys. Rev. Lett. **35**, 1619 (1975).
[132] J. M. Reinartz and A. Dymanus, Chem. Phys. Lett. **24**, 346 (1974).
[133] P. B. Davies, R. M. Neumann, S. C. Wofsy, and W. Klemperer, J. Chem. Phys. **55**, 3564 (1971).

[134]S. I. Chan, M. R. Baker, and N. F. Ramsey, Phys. Rev. **136**, A1224 (1964).
[135]G. Cazzoli, C. Puzzarini, M. E. Harding, and J. Gauss, Chem. Phys. Lett. **473**, 21 (2009).
[136]W. L. Ebenstein and J. S. Muenter, J. Chem. Phys. **80**, 3989 (1984).
[137]G. Cazzoli and C. Puzzarini, J. Mol. Spectrosc. **233**, 280 (2005).
[138]R. J. Butcher, B. Saubaméa, and C. Chardonnet, J. Mol. Spectrosc. **188**, 142 (1998).
[139]B. Fabricant, D. Krieger, and J. S. Muenter, J. Chem. Phys. **67**, 1576 (1977).
[140]W. M. Itano and I. Ozier, J. Chem. Phys. **72**, 3700 (1980).
[141]S. C. Wofsy, J. S. Muenter, and W. Klemperer, J. Chem. Phys. **55**, 2014 (1971).
[142]D. H. Sutter and H. Dreizler, Z. Naturforsch. **A 56**, 425 (2001).
[143]R. E. Cupp, R. A. Kempf, and J. J. Gallagher, Phys. Rev. **171**, 60 (1968).
[144]A. H. Saleck, M. Tanimoto, S. P. Belov, T. Klaus, and G. Winnewisser, J. Mol. Spectrosc. **171**, 481 (1995).
[145]L. Bizzocchi, C. Degli Eposti, L. Dore, and C. Puzzarini, Chem. Phys. Lett. **408**, 13 (2005).
[146]R. D. Brown, P. D. Godfrey, D. McNaughton, A. P. Pierlot, and W. H. Taylor, J. Mol. Spectrosc. **140**, 340 (1990).
[147]E. Rothstein, J. Chem. Phys. **50**, 1899 (1968).
[148]J. M. L. J. Reinartz, W. L. Meerts, and A. Dymanus, Chem. Phys. **31**, 19 (1978).
[149]F. H. De Leeuw and A. Dymanus, Chem. Phys. Lett. **7**, 288 (1970).
[150]W. H. Flygare, J. Chem. Phys. **42**, 1157 (1965).
[151]H. S. P. Müller, J. Farhoomand, E. A. Cohen, B. Brupbacher-Gatehouse, M. Schäfer, A. Bauder, and G. Winnewisser, J. Mol. Spectrosc. **201**, 1 (2000).
[152]T. W. Keal and D. J. Tozer, J. Chem. Phys. **121**, 5654 (2004).
[153]G. Vignale and M. Rasolt, Phys. Rev. Lett. **59**, 2360 (1987).
[154]G. Vignale and M. Rasolt, Phys. Rev. B **37**, 10685 (1988).
[155]G. Vignale, M. Rasolt, and D. J. W. Geldart, Phys. Rev. B **37**, 2502 (1988).
[156]G. Vignale, M. Rasolt, and D. J. W. Geldart, Adv. Quanutm Chem. **21**, 235 (1990).
[157]A. M. Lee, N. C. Handy, and S. M. Colwell, J. Chem. Phys. **103**, 10095 (1995).
[158]J. Tao and J. P. Perdew, Phys. Rev. Lett. **95**, 196403 (2005).
[159]J. Tao and G. Vignale, Phys. Rev. **B 74**, 193108 (2006).
[160]K. Higuchi and M. Higuchi, Phys. Rev. **B 74**, 195122 (2006).